JOURNAL OF AIRCRAFT
Vol. 45, No. 4, July–August 2008

Interactive Inverse Design Optimization of Fuselage Shape for Low-Boom Supersonic Concepts

Wu Li*
NASA Langley Research Center, Hampton, Virginia 23681
Elwood Shields†
Alliant Techsystems, Inc., Hampton, Virginia 23681
and
Daniel Le‡
University of Virginia, Charlottesville, Virginia 22904

DOI: 10.2514/1.35543

This paper introduces a tool for boom optimization using smoothest shape modifications. This tool allows interactive inverse design optimization to develop a fuselage shape that yields a low-boom aircraft configuration. A fundamental reason for developing this boom optimization tool is the need to generate feasible low-boom conceptual designs that are appropriate for further refinement using computational-fluid-dynamics-based preliminary design methods. The boom optimization tool was not developed to provide a numerical solution to the inverse design problem. Instead, it was intended to help designers find the right configuration among an infinite number of possible configurations that are equally good using any numerical figure of merit. This boom optimization tool uses the smoothest shape modification strategy for modifying the fuselage radius distribution at 100 or more longitudinal locations to find a smooth fuselage shape, which reduces the discrepancies between the design and target equivalent area distributions over any specified range of effective distance. For any given supersonic concept (with wing, fuselage, nacelles, tails, and/or canards), a designer can examine the differences between the design and target equivalent areas, decide which part of the design equivalent area curve needs to be modified, choose a desirable rate for the reduction of the discrepancies over the specified range, and select a parameter for smoothness control of the fuselage shape. The boom optimization tool will then generate a fuselage shape based on the designer's inputs in a matter of seconds. Using this tool, within a few hours, a designer can either generate a realistic fuselage shape that yields a supersonic configuration with a low-boom ground signature or quickly eliminate any configuration that cannot achieve low-boom characteristics with fuselage shaping alone. A conceptual design case study is documented to demonstrate how this boom optimization tool can be used to develop a low-boom supersonic concept from a low-drag supersonic concept. The paper also contains a study on how perturbations in the equivalent area distribution affect the ground signature shape and how new target area distributions for low-boom signatures can be constructed using superposition of equivalent area distributions derived from the Seebass–George–Darden theory.

Nomenclature

A	=	normal area
A_e	=	equivalent area
$\langle \mathbf{a}, \mathbf{b} \rangle$	=	dot product of two vectors **a** and **b**
$f(x)$	=	camber location of fuselage at x
$G(\mathbf{r})$	=	least-squares error of mismatch of equivalent areas for given **r**
$L(\mathbf{r})$	=	linear term in Taylor expansion of $G(\mathbf{r})$
l	=	total length of fuselage
l_e	=	effective length of aircraft
$\mathbf{r}$	=	vector of radii at a finite number of x locations
$r(x)$	=	radius of a circular cross section of fuselage at x
s	=	smoothness control parameter for fuselage shape modifications
x_e	=	effective distance along the longitudinal direction
x, y, z	=	coordinates of a point in space
ΔA	=	change in area
$\Delta r(x)$	=	change in radius at x
$\Delta r''(x)$	=	second derivative of $\Delta r(x)$
$\Delta r^{(3)}(x)$	=	third derivative of $\Delta r(x)$
δ	=	positive constant bound for $\Delta r^{(3)}(x)$
$(\partial G/\partial \mathbf{r})(\mathbf{r}_k)$	=	gradient vector of $G(\mathbf{r})$ with respect to **r** evaluated at $\mathbf{r}_k$
$\mathcal{E}$	=	envelope region generated by low-boom equivalent area distributions
λ_s	=	positive multiple of bound for $\Delta r^{(3)}(x)$
ρ	=	reduction rate of $G(\mathbf{r})$ in boom optimization tool

Subscripts and Superscripts

i	=	index for ith component of vector
k	=	index for an instance of vector **r**
m	=	number of x_e locations for A_e distributions
n	=	number of fuselage cross sections

Presented as Paper 0136 at the 46th AIAA Aerospace Sciences Meeting and Exhibit, Reno, NV, 7–10 January 2008; received 7 November 2007; revision received 15 January 2008; accepted for publication 26 January 2008.

*Senior Research Engineer, Aeronautics Systems Analysis Branch; w.li@nasa.gov.
†Senior System Engineer, Space Division.
‡Graduate Research Assistant, Mechanical and Aerospace Engineering; currently NASA Langley Research Center, Mail Stop 442, Hampton, Virginia 23681. Member AIAA.

I. Introduction

MANY research papers address how to design a supersonic configuration that has desirable low-boom characteristics as determined by the Seebass–George–Darden (SGD) boom minimization theory [1–3]. The low-boom signatures predicted by the SGD theory could be realized by wing–fuselage configurations. However, for a given low-boom signature generated by the SGD theory, the question still exists for whether one could develop a feasible aircraft configuration with nacelles and tails that has a low-boom ground signature similar to that predicted by the SGD theory. In this paper, Whitham's boom propagation method [4,5] is used for boom signature analysis.

Past attempts have demonstrated little success in creating feasible aircraft configurations with nacelles and tails that have a total equivalent area distribution matching one of the target A_e distributions derived from the SGD theory. Essentially, three design methods exist for generating a supersonic concept with a shaped boom ground signature: 1) use a direct optimization method that minimizes numerical figures of merit for low-boom characteristics, 2) construct new, "realizable" target equivalent area distributions (or target near-field pressure distributions) that result in shaped boom ground signatures, and 3) develop new tools to help designers find acceptable low-boom configurations. Many unsuccessful attempts have been made using the first two methods to obtain supersonic configurations that have shaped boom ground signatures. In this paper, we introduce a tool called BOSS (boom optimization using smoothest shape modifications) for interactive inverse design optimization of fuselage shape for developing low-boom concepts and demonstrate how it could help designers develop realistic aircraft concepts with low-boom ground signatures.

McMasters and Cummings point out the need for developing optimization strategies "that may be unique to the aircraft industry, which take advantage of the assumptions and techniques that airplane designers use, rather than letting a computer churn away and come up with theoretically possible, but practically impossible, configurations" (see [6], p. 14). BOSS is not developed to provide a numerical solution to the inverse design problem. Instead, BOSS tries to help designers find the "right" configuration among an infinite number of possible configurations that are essentially equal using any numerical figure of merit.

This paper is organized as follows. Secs. II, III, and IV provide a brief survey of various numerical methods for design of low-boom supersonic concepts: inverse design by matching A_e distributions, inverse design by matching near-field pressure distributions, and numerical optimization for sonic-boom minimization. The interactive inverse design process for low-boom supersonic concepts using BOSS is discussed in Sec. V. To demonstrate how BOSS can assist conceptual designers in generating low-boom concepts, Sec. VI includes a case study that demonstrates the application of BOSS in developing a low-boom supersonic concept from a low-drag supersonic concept. In Sec. VII, we attempt to understand why similarly shaped boom signatures can have different A_e distributions and why "sawtooth" oscillations in boom signature are unavoidable. Concluding remarks are given in Sec. VIII.

II. Inverse Design by Matching Equivalent Area Distributions

The SGD boom minimization theory [1–3] can be used to generate A_e distributions that minimize sonic boom on the ground when analyzed using Whitham's boom propagation method [4,5]. Darden's main contributions are the extension of Seebass and George's theory from a uniform and isothermal atmosphere to a real atmosphere [2] and a more flexible form of Seebass and George's F function, which allows a low-boom configuration with a sharper nose, rather than the blunt nose required by Seebass and George's theory [3]. In Fig. 8 of [3], for a body of revolution, Darden showed that drag caused by nose bluntness can be reduced with a marginal increase of the sonic-boom pressure strength. Seebass and Argrow [7] gave a comprehensive review of the historical development of the SGD theory and called it the classical Jones–Seebass–George–Darden theory. Most studies on inverse design of low-boom concepts are based on Darden's area distribution for a ramp ground signature (see [8–14]).

Two empirical modifications of the sonic-boom-minimizing F functions were made to incorporate some practical considerations in design of low-boom configurations. The first is a hybrid combination of flattop and ramp F functions. For the same initial overpressure level, it was observed that ramp signatures lead to a shorter supersonic aircraft, whereas flattop signatures are less sensitive to atmospheric changes in temperature [15,16] (see also [17], p. 3). To capture the benefits of both flattop and ramp signatures, Haglund developed [15,16] a hybrid F function for sonic-boom minimization. The ground signature for a hybrid F function has a flat segment near the initial pressure peak, followed by a ramp (see Fig. 1a). The second modification is to use a conical fuselage nose [18] instead of the cusp-shaped fuselage nose used by Darden [3]. These modifications provide additional flexibilities for conceptual design of low-boom configurations (see [18]). For example, the hybrid F function allows designers to do tradeoffs between the initial overpressure and the maximum overpressure in the ground signature, as well as the shape of the target equivalent area distribution. Figure 1a shows ramp, hybrid, and flattop signatures using the following parameters of F functions defined in [18]: effective length l_e of 111 ft, the fuselage nose-cone length y_f of 6 ft, ramp slope of 0.35, beginning-cruise weight of 96,500 lb, cruise altitude of 53,000 ft, and cruise Mach of 1.8. For this set of parameter values, if both the initial overpressure and the maximum overpressure are used as the figures of merit, then the ramp and flattop signatures become two endpoints of a Pareto frontier (see Fig. 2). The hybrid signatures fill the Pareto frontier if the length of the flat segment in the hybrid signature is varied (see Fig. 1a).

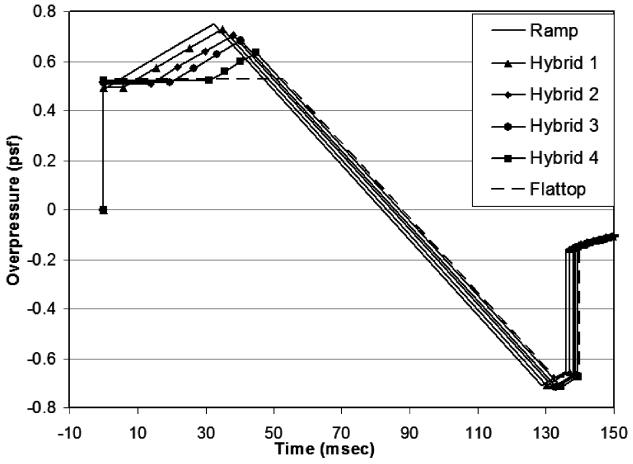

a) Comparison of signatures

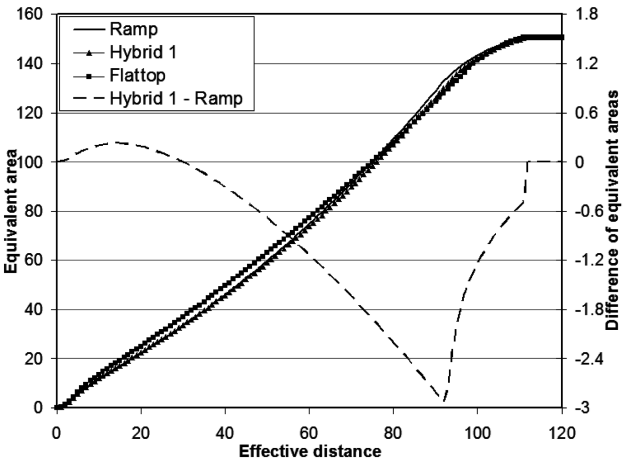

b) Comparison of equivalent areas

Fig. 1 Ramp, hybrid, and flattop ground signatures and the corresponding area distributions.

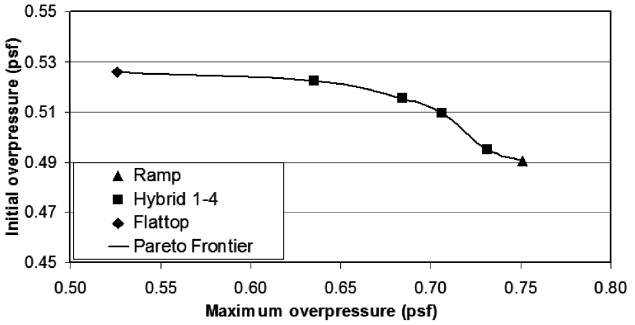

Fig. 2 Pareto frontier for initial and maximum overpressures of flattop, ramp, and hybrid signatures.

The hybrid equivalent area in Fig. 1b corresponds to the hybrid point with an initial overpressure of 0.496 psf in Fig. 2 or hybrid 1 in Fig. 1a and is assumed to have the potential benefit of maintaining the level of the initial overpressure under atmospheric perturbations [16] in comparison with the ramp signature. However, in reality, because the difference between the A_e distributions of the ramp and the hybrid signatures is quite small (see the secondary axis for the difference between the two area distributions in Fig. 1b), one might wonder whether such a difference would make any meaningful impact on the shape of the low-boom configuration. We will come back to this issue in the discussion of a low-boom configuration that is designed for the hybrid signature.

Shepard and Sullivan [19] investigated the relationship between sonic-boom shapes and loudness. The main conclusion is that, among all of the boom signatures with the same maximum overpressure and rise time, the subjective loudness levels of the flattop signature and the *N* wave are nearly the same, whereas the ramp and the hybrid signatures have lower loudness levels. Therefore, for tradeoff studies of sonic-boom shapes during conceptual design, a comparison of loudness levels for various sonic-boom shapes that correspond to the Pareto points in Fig. 2 is more useful and provides insight into pros and cons of different sonic-boom shapes under the same set of design constraints. For all of the signatures in Fig. 1a, the loudness levels are in the range of 85.3–85.9 PLdB (perceived loudness level).

Low-boom supersonic configurations that correspond to theoretical boom signatures could still be too long to be practical (e.g., see [20]). In an attempt to develop low-boom configurations with a reasonable length for supersonic business jets, Mack first proposed the idea of allowing a difference between the maximum equivalent area due to lift and the maximum equivalent area based on the boom minimization theory [21]. This approach allows a shaped boom signature with a more practical configuration, at the expense of an increase in aftbody sonic-boom pressure strength when predicted by Whitham's *F*-function method [4,5]. Mack discussed extensively the difficulties of designing a low-boom supersonic business jet (see [21], p. 21). Significant differences were evident between the target hybrid ground signature and the predicted ground signature of the proposed low-boom supersonic business concept, even without nacelles (see [21], Fig 13). A wind-tunnel model was constructed based on a watertight version of the conceptual design; the model was tested in the Langley Unitary Plan Wind Tunnel (see [22], p. 6) and analyzed by Choi et al. [22]. The ground signatures of the wind-tunnel model, propagated from the measured near-field pressures by PCBoom3, are *N* waves; the ground signatures of the wind-tunnel model, propagated from predicted near-field pressures, have a two-level staircase-type shape near the initial peak (see [22], Figs. 17–19).

Numerical algorithms were proposed to modify the fuselage shape so that the total A_e distribution of the resultant configuration matches a target area distribution. Barger and Adams's methods [23] were based on a fixed-point iteration procedure for changing the fuselage so that the equivalent area of the fuselage volume matches a target distribution. Barger and Adams developed two numerical algorithms. One algorithm is slow to converge and has difficulty matching the target area distribution but generates a smooth fuselage; the other one converges quickly but generates a wavy fuselage that more closely matches the target area distribution. As an example, they constructed two different fuselage shapes with circular cross sections that have the same target area distribution (see [23], Figs. 4, 5). Their study has some negative implications on numerical algorithms for modifying fuselage shapes to match a target area distribution: the algorithm might numerically generate a fuselage shape that either does not match the target area distribution or is not realistic.

Rather than developing an algorithm for numerical fuselage solutions for equivalent area matching, Mack and Needleman [24] used a semi-empirical method for modifying the fuselage radius distribution to match the target A_e distribution. This method could have significant errors if the fuselage violates the slender-body assumption (i.e., a relatively flat camber line and small variations in fuselage radius distribution). This semi-empirical method was used to generate various low-boom supersonic concepts, but additional experience-based area trimming might be required to obtain a desirable low-boom configuration (see [21,24]).

Recently, Rallabhandi and Mavris [25] tried a new approach for low-boom supersonic conceptual design. A new flexible form of the *F* function was used to generate new target A_e distributions for sonic-boom minimization. The fuselage shape was then modified to meet the nose shape. After a suitable match was obtained, the fuselage shape was frozen and the other components were perturbed to match the target area distribution as closely as possible. However, this approach could not obtain a supersonic concept for which the total equivalent area was a desirable match to the target area distribution (see [25], Fig. 25). In the same paper [25], a parallel genetic algorithm was used to find low-boom supersonic concepts, but no specific shape parameters were given.

III. Inverse Design by Matching Near-Field Pressure Distributions

The limitations of Whitham's *F*-function method for sonic-boom prediction are well known (see, for example, [26]). A remedy is to use a three-dimensional flow solver to predict the near-field pressure distributions and then extrapolate the near-field pressure distributions to the ground using either Thomas's code [27] or PCBOOM [28].

Inverse design processes for fuselage shaping of low-boom supersonic concepts, coupled with computational fluid dynamics (CFD) analysis to match near-field pressure targets, have been studied for many years (see [10–12,14,20,29,30]).

Makino et al. [10] studied a wing-body configuration based on Darden's target area distribution [3] for a flattop ground signature with a blunt nose (see the section on aircraft configuration in [10]). Figure 8 in [10] shows an almost perfect match of the configuration's A_e distribution and the target, everywhere except near the end of the configuration. The predicted ground signature is generated by Thomas's code [27] using a near-field pressure distribution at six body lengths below the configuration. Significant differences are seen between the predicted ground signature and the target flattop ground signature (see [10], Fig. 11). Specifically, the predicted maximum overpressure is 2.0 psf instead of 1.0 psf for the target signature. No information is provided on the ground signature predicted by Whitham's *F*-function method.

Later, Makino et al. [29] used numerical optimization of fuselage geometry of the low-boom baseline discussed in [10] to modify the sonic-boom signature predicted by Thomas's code [27] using a near-field pressure distribution at six body lengths. Makino et al. [29] used numerical optimization to modify the fuselage shape over a selected segment of the fuselage. This process was repeated several times over different segments of the fuselage. The design variables of the optimization problem were eight control points of a *B*-spline representation of the shape of the fuselage segment that was being modified (see [29], p. 672 for details). This effort is the first to show that a combination of heuristics (e.g., segment selection and choice of design variables) and numerical optimization could be useful for inverse design of low-boom configurations by matching a target near-field pressure distribution.

Nadarajah et al. [31] used an adjoint method to shape a wing-body configuration to match a target near-field pressure distribution. They were able to reduce the sonic-boom level with a significant drag penalty. They then tried a composition of the drag coefficient and the pressure difference as the objective function for shape optimization using the adjoint method, and showed that the method could reduce the peak pressures while maintaining the drag coefficient at the same level. However, the adjoint method could not generate a configuration with shaped boom signatures such as ramp or flattop signatures.

The only flight validation of any shaped boom signature is the modified F-5E shaped sonic boom demonstrator aircraft, which was designed with an initial configuration obtained by matching A_e distributions, followed by an iterative inverse design process of matching a target near-field pressure distribution. Here is a description of the design process [14]:

> Initially, linear analysis tools were used to design the geometry shape of the aircraft to achieve the designed off-body pressures (changes to the area distribution). This geometry was then analyzed with high-order CFD to compute the resultant off-body pressure signature of the candidate geometry. This became an iterative process, of geometry modifications, CFD analysis of geometry to compute pressure signatures, and then modifications of the geometry again.

The final design is an innovative configuration with great knowledge and experience behind it. Flight tests validated that the modified F-5E had a shaped sonic-boom signature vs the *N*-wave signature of the baseline F-5E [32]. The tests demonstrated for the first time that specialized aircraft shaping techniques can be used to tailor the sonic-boom ground signature. (See [33] for the origin and history of the shaped sonic-boom demonstrator project.) Note that the shaping techniques only produced a set of candidate geometry shapes, and the wind-tunnel model shape was determined by consensus of a working group [33].

IV. Numerical Optimization for Sonic-Boom Minimization

There have been many studies on how to use direct optimization methods for generating low-boom configurations [13,31,34–39]. An open question is "What objective function could lead to an optimal solution having a shaped boom signature with a low level of loudness?" Various forms of objective functions, including the initial overpressure, perceived loudness, drag, and so on, were proposed. Although each method is able to generate a better configuration in terms of the chosen objective function, no evidence indicates that any optimized configuration has a shaped low-boom signature except the configurations generated by Makino and Kroo [39].

Makino and Kroo [39] used a signature mold line evaluation method to seek a configuration with a low-boom ground signature. The documented process uses 12 design variables and genetic algorithms for shaping a low-drag configuration into a configuration for which the ground signature is within the mold lines of the target signature and the overpressure is equal to the minimum absolute value. Makino and Kroo were able to generate three configurations that have flattop, ramp, and hybrid signatures, respectively. The method is not a traditional inverse design based on the target equivalent area, but it can be considered a novel inverse design method for matching the envelope of the ground signature or the target signature mold lines. While experience indicates that many variables are needed to define a large design space a priori that contains configurations with low-boom ground signatures, Makino and Kroo used surprisingly few design variables to generate configurations with different low-boom characteristics.

V. Interactive Optimization for Matching Equivalent Area Distributions

In open literature, few references exist that document what and how design variables are modified to generate a low-boom configuration for a target area or pressure distribution (see, for example, [14,20,21,23,29]). The most detailed description was given by Makino et al. [29], who used 14 numerical optimization iterations to modify eight control points of a *B*-spline representation of the fuselage geometry over the selected segments of the fuselage. Recently, Makino and Kroo [39] used an Akima-spline representation of the radius distribution of an axisymmetric fuselage with seven control points for sonic-boom minimization using genetic algorithms. Their work showed very promising results for shaped boom configurations with tails and nacelles. One significant contribution of this work is the demonstration that, with an appropriate combination of the objective function and the design space parameterization, one could use a numerical optimization method to generate configurations with shaped boom signatures. However, one practical difficulty of using Makino and Kroo's optimization method is the choice of design variables and their ranges. Makino and Kroo stated in Sec. 2 of [39] that "the ranges of the design variables are specified so that they can represent both low-drag and low-boom configurations while they are kept as small as possible for fast design convergence." In practice, identifying a priori the parametric design space that will include low-boom configurations is nearly impossible.

Because of the difficulty of designing a reasonably well-blended wing–body supersonic configuration for high-fidelity CFD analysis, the current conceptual design framework at Langley Research Center is based on a modified linear solution of forces and moments acting on twisted and cambered lifting surfaces of arbitrary planform for aerodynamic analysis and classical sonic-boom minimization theory for low-boom configuration design.

For a complete supersonic configuration with tails and nacelles, considerable time and effort is generally required to develop a low-boom configuration with some kind of practical considerations such as mission requirements. After overcoming the initial challenges of designing an aircraft layout, such as wing planform and nacelle locations (see, for example, [20,21]), one might find that the resulting configuration cannot be modified to match the target A_e distribution due to lack of volume between the target distribution and the equivalent area distribution due to lift. Several iterations are required before one gets a supersonic configuration that could be reshaped as a low-boom configuration. With this semi-empirical method [24], a considerable amount of time can be spent shaping the fuselage to achieve relatively good agreement between the configuration's area distribution and the target, such as shown in Fig. 9 of [21]. However, significant differences can still exist between the corresponding ground signatures (see [21], Fig. 13). A similar mismatch between the configuration's A_e distribution and the target were also reported in [20] because of the nacelles.

In this paper, we will only focus on developing an interactive optimization method for solving the inverse design problem of modifying the fuselage geometry to match a given target A_e distribution. In principle, the method is also applicable for solving the inverse design problem of modifying the fuselage geometry for a given near-field pressure distribution. The goal is to develop a practical optimization procedure for fuselage shaping that designers could use to develop low-boom concepts quickly, with a turnaround time of days instead of months, without any prior knowledge of any appropriate parameterization of the design space.

A. Sonic-Boom Analysis Framework

For a given beginning-cruise weight, cruise altitude, cruise Mach, initial overpressure, and two parameters defining the ground signature shape (the length of the flattop and the slope of the ramp), the sonic-boom minimization code Hybrid [16] can generate a target A_e distribution for a configuration with a conic fuselage nose [18] and minimum effective length. When other parameters are fixed, as the length of flattop is increased, either the effective length increases or the initial overpressure increases. The boom signatures shown in Fig. 1a were generated by changing the length of the flattop while fixing the effective length.

Aircraft geometry is defined by six aircraft components: fuselage, wing, nacelle (one circular shell and one pylon), and *T* tail

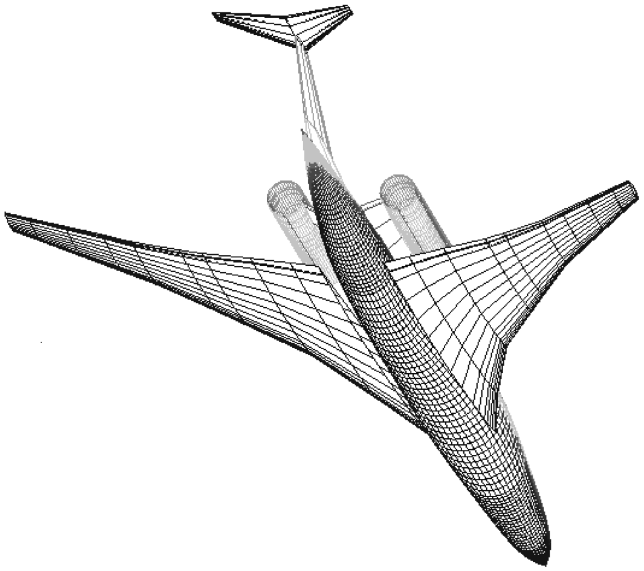

Fig. 3 Aircraft geometry defined by grid points.

(one vertical tail and one horizontal tail), with no definition of intersections. Each component is defined by a fixed number of cross sections with a fixed number of points on each cross section (see Fig. 3). An analytical surface form of each component can be generated by a *B*-spline interpolation of the grid points, but we use the piecewise linear interpolation for surface points between the given grid points because it is sufficient for numerical calculation of the equivalent areas. If enough grid points are used, then the difference between a *B*-spline surface representation and the piecewise linear interpolation is negligible.

In this paper, we only consider fuselages with circular cross sections. A circular fuselage is defined by a camber line $z = f(x)$ and a radius distribution $z = r(x)$. The fuselage surface points (x, y, z) satisfy the equation $y^2 + [z - f(x)]^2 = r(x)^2$. Of course, the graphs of $z = f(x)$ and $z = r(x)$ are piecewise linear interpolants of the given data sets $\{(x_0, f(x_0)), (x_1, f(x_1)), \ldots, (x_n, f(x_n))\}$ and

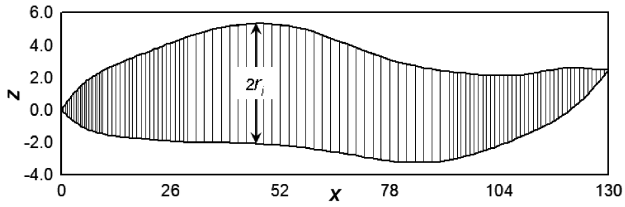

Fig. 4 Side view of fuselage geometry defined by circular cross sections.

$\{(x_0, r_0), (x_1, r_1), \ldots, (x_n, r_n)\}$, respectively. Figure 4 shows a side view of the fuselage geometry. Note that the top and bottom surfaces are defined by $z_u = f(x) + r(x)$ and $z_l = f(x) - r(x)$, respectively. The camber line is designed to achieve three purposes:

1) At the cruise angle of attack, the front part of the fuselage behaves essentially like a body of revolution along the stream line.

2) The cabin floor angle will be within some acceptable limits.

3) The aft part of the fuselage camber increases the effective length of the configuration and enhances ground clearance during rotation for takeoff and landing.

These are knowledge-based practical considerations for a credible aircraft configuration.

AWAVE [40] is used to evaluate the equivalent area distribution due to volume, and a modified linear method [41] is used to evaluate the longitudinal lift distribution. These distributions are then used by PBOOM [42] to evaluate the sonic-boom ground signature of the configuration.

A ModelCenter [43] wrapper of the sonic-boom analysis was implemented by Ozoroski and Geiselhart of Aeronautics Systems Analysis Branch at NASA Langley Research Center. This wrapper is used as the basis for developing the current interactive inverse design optimization process for low-boom concepts.

The current low-boom conceptual design process first determines a layout for all of the components, designs a wing that sufficiently satisfies mission requirements, and then reshapes the fuselage (by modifying the discrete radius distribution r_i, as shown in Fig. 4) to achieve a low-boom configuration. Figure 5 shows the ModelCenter [43] layout of the analysis and optimization tools used in the low-boom conceptual design process.

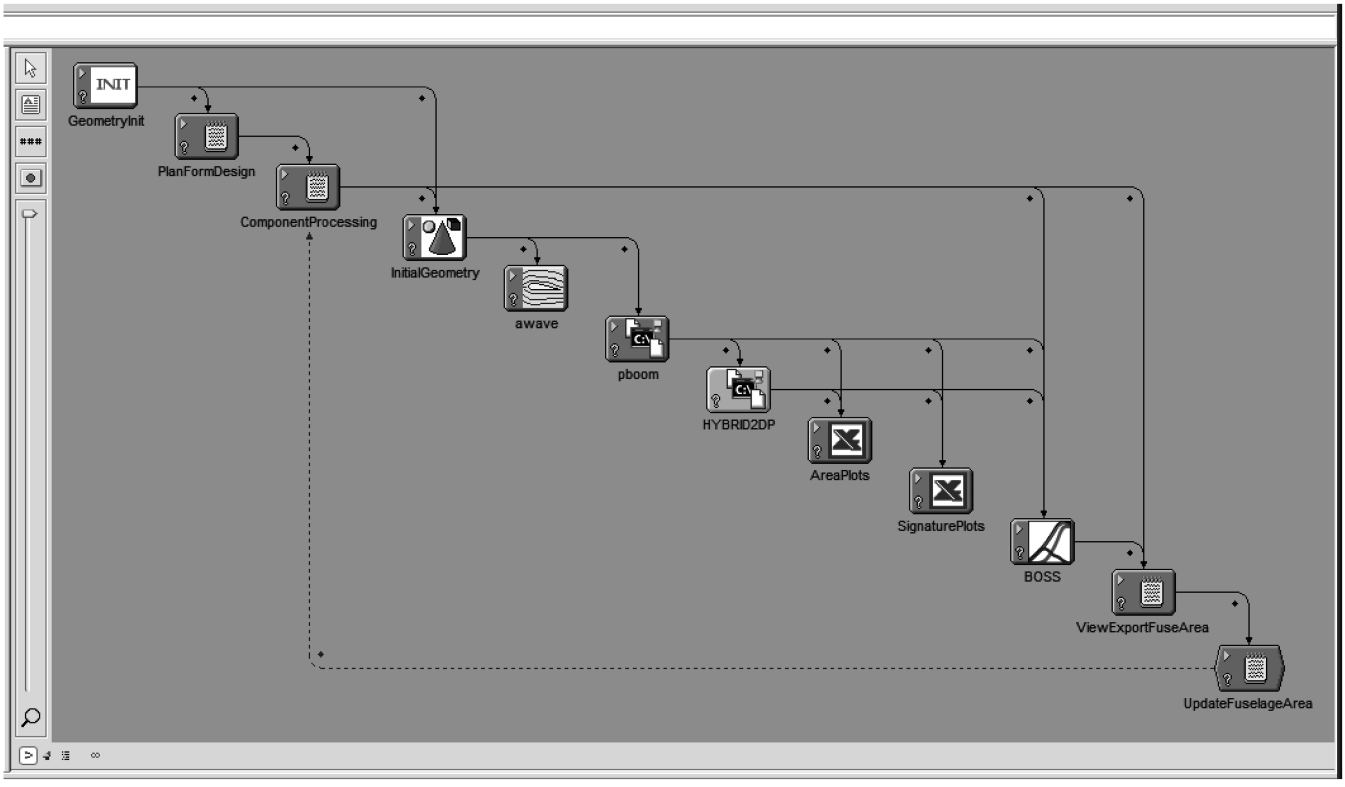

Fig. 5 ModelCenter layout of the low-boom conceptual design process.

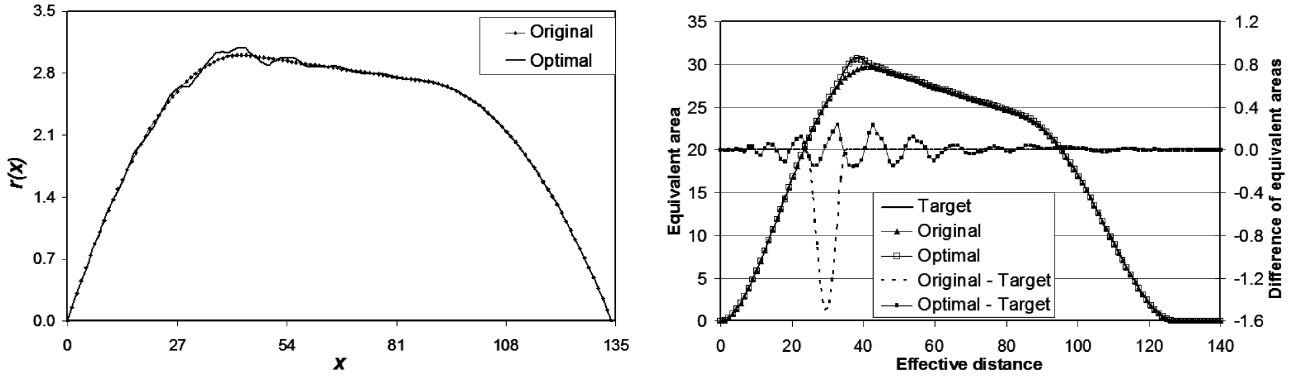

a) Comparison of fuselage radii b) Comparison of equivalent areas

Fig. 6 Fuselage shapes and A_e distributions for the oscillatory case.

B. Intrinsic Difficulties of Matching Equivalent Areas

We shall use two numerical examples to illustrate the difficulties of finding an axisymmetric fuselage for which the A_e distribution matches a given target distribution. The first example shows a smooth target A_e distribution that cannot be matched by the equivalent area of any nonoscillatory fuselage shape; the second example shows that one smooth fuselage and another oscillatory fuselage have the same smooth A_e distribution. In this subsection, the equivalent area is computed under the assumptions that the cruise $M = 1.8$ and the fuselage is at an angle of attack of 1.94 deg. The fuselage geometry is defined by its radius distribution at 120 equally spaced longitudinal locations.

The radius distribution of an axisymmetric fuselage is defined as follows: $r(0) = r(135) = 0$, $r(45) = 3$, $r(90) = 2.7$; $r(x)$ is a quadratic function for $0 \le x \le 45$, $r(x)$ is a linear function for $45 \le x \le 90$; $r(x)$ is a quadratic function for $90 \le x \le 135$; and $r(x)$ has continuous first derivatives at $x = 45$ and $x = 90$. This radius distribution is plotted as "original" in Fig. 6a. Then a target equivalent area distribution is generated as follows: $A_{e,\text{target}}(x) = A_e(x) + \Delta A(x)$, where $A_e(x)$ is the A_e distribution of the original fuselage and $\Delta A(x) = 0.0384(x - 35)^2(x - 40)^2$ if $35 \le x \le 40$ and $\Delta A(x) = 0$ otherwise. An optimal fuselage is obtained by using a numerical optimization code that modifies the original fuselage for matching the A_e distributions.

Figure 6b shows the A_e distributions for the original and optimal fuselages, as well as the target distribution. Note that the distribution for the optimal fuselage closely matches the target distribution, with maximum error equaling about 0.3 (see the secondary axis in Fig. 6b for the area difference). This value is about 1% for the relative fitting error. However, the optimal fuselage is quite oscillatory. The oscillations are intrinsic in this case. To match the target A_e distribution, the fuselage radii must increase over the range $35 < x < 40$, which force the radii just before $x = 35$ and after $x = 40$ to decrease so that the equivalent areas for these x values will not change. These changes lead to a wavelike effect on the fuselage shape (see Fig. 6a). In other words, if the difference between the current and target A_e distributions is a local bump, then oscillatory shape modifications may be necessary for matching the equivalent area distributions.

In the second example, the target A_e distribution is defined as follows: $A_{e,\text{target}}(x) = A_e(x) + \Delta A(x)$, where $A_e(x)$ is the A_e distribution of the original fuselage, $\Delta A(x) = 0.000005(x - 35)^2 (x - 95)^2$ if $35 \le x \le 95$ and $\Delta A(x) = 0$ otherwise. The same numerical optimization code is used for matching the A_e distributions with two different initial guesses. The first initial guess is a fuselage for which the radius distribution is defined as $\sqrt{A_{e,\text{target}}(x)/\pi}$, and the second initial guess is the original fuselage. The two initial guesses lead to two different fuselages, labeled "solution 1" and "solution 2" in Fig. 7a, for which the equivalent area distributions are in very good agreement with the target distribution (see the secondary axis in Fig. 7b for the area difference).

The matching errors in Fig. 7b suggest that solution 1 is not as optimal as solution 2. However, the maximum matching error of 0.2 for solution 1 is smaller than the 0.3 seen in the previous example. Without knowing the existence of solution 2, one might be more than willing to accept such a good match of the equivalent area distributions. The obvious kinks in the radius distribution for solution 1 (see Fig. 7a) suggest that a large number of design variables for fuselage geometry modifications might lead to unnecessary oscillations in the fuselage shape. In this case, both the radius and A_e distributions are evaluated at 120 equally spaced locations between 0 and 135. Barger and Adams [23] had a more dramatic example of one smooth and one oscillatory fuselage with the same A_e distribution evaluated at 27 locations. These examples indicate that the inverse problem of matching A_e distributions could have multiple solutions.

C. Smoothest Shape Modifications

Two approaches can be used to avoid the difficulties illustrated in the previous subsection. The first one is to use a spline parametric representation of the fuselage radius distribution with a few (5–8)

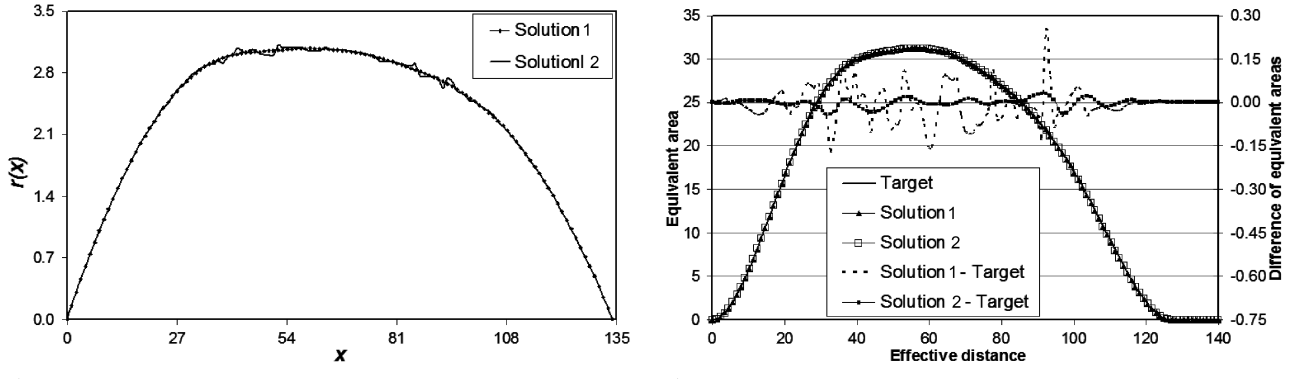

a) Comparison of fuselage radii b) Comparison of equivalent areas

Fig. 7 Fuselage shapes and A_e distributions for the multiple solution case.

control points [29,36–39]. For a complex configuration, such a parametric representation of fuselage radius distribution may be inadequate for fuselage shaping to match a target A_e distribution. In a case where a desirable fuselage shape could not be obtained, one would be left with lingering doubts whether the design space is large enough to include the right solution. In many cases, the choice of parametric forms for the design space determines whether or not a numerically optimal solution yields a meaningful design. The second approach is to allow almost arbitrary modifications of the fuselage shape, but the optimization algorithm only seeks the smoothest modification for design improvement iteratively. A successful application of this strategy has been demonstrated for transonic airfoil shape optimization [44].

Note that fuselage shape change can be facilitated by a change in $r(x)$, denoted by $\Delta r(x)$. An important issue is identifying a criterion to be used for desirable design improvements during optimization iterations. For numerical minimization problems, two basic strategies determine the desirable modifications for gradient-based optimization methods. The first is based on some numerical convergence rule, and the modifications are made to achieve fast convergence to a local minimum solution (such as Newton methods). These types of methods usually do not work well for complex engineering design optimization problems as a result of numerical errors in the sensitivity calculations of those functions for which the values are generated by computer codes. The second strategy is to find a modification that achieves the greatest reduction of the objective function value in each iteration, such as the steep descent method, and terminates if no design improvement can be made. In our limited experience, this type of method only works when an appropriate parametric design space is used. Many examples can be found in literature about unrealistic but numerically optimal solutions of shape optimization problems. In practice, no mathematical model could cover all of the physics related to aircraft. System analysts are well aware that numerical optimization methods tend to generate impractical or even absurd concepts.

The smoothest shape modification [44] can also be considered as an optimization strategy, based on the following two principles: 1) smoother shape modifications are more desirable than oscillatory ones, and 2) smaller shape modifications are more reliable than larger ones if they have the same predicted reduction of the objective function. Although the first principle does not require much explanation, the second one needs some justification. In general, among the feasible modifications that achieve the same predicted reduction of the objective function, the smallest shape modification has the best chance of actually reducing the value of the objective function because the prediction error of a linear Taylor approximation increases as the magnitude of the shape modifications increases. Moreover, the second principle helps to eliminate unnecessary and random shape modifications (perhaps one major reason for unrealistic optimal shapes when the number of design variables is large) and makes the modifications more relevant to desirable performance improvement based on simulation models.

To define the smoothest shape modification scheme for fuselage shape optimization, we use a cubic B-spline interpolation $z = r(x)$ of the discrete fuselage radius distribution $(x_0, r_0), (x_1, r_1), \ldots, (x_n, r_n)$, where $0 = x_0 < x_1 < \ldots < x_n = l$ (the length of the fuselage). Then, fuselage shape modifications can be represented by a cubic B-spline $\Delta r(x)$ with knots at $x_0, x_1, \ldots, x_n$.

The third derivative $\Delta r^{(3)}(x)$ of $\Delta r(x)$ is a piecewise constant function. That is,

$$\Delta r^{(3)}(x) = \Delta r_i^{(3)} \quad \text{for } x_{i-1} < x < x_i, \qquad 1 \le i \le n \tag{1}$$

where $\Delta r_i^{(3)}$ are scalars. From Eq. (1), one can impose an upper bound δ on $|\Delta r^{(3)}(x)|$ for all x by using the following system of linear inequalities:

$$-\delta \le \Delta r^{(3)}\left(\frac{x_{i-1} + x_i}{2}\right) \le \delta \quad \text{for } 1 \le i \le n \tag{2}$$

Note that the radii at the fuselage nose and tail are zero, and so $r(x_0) = r(x_n) = \Delta r(x_0) = \Delta r(x_n) = 0$. If $\delta = 0$, then $\Delta r^{(3)}(x) = 0$ or $\Delta r(x)$ is a quadratic function, which results in a very smooth but not necessarily small shape modification. In fact, if $\Delta r(x) = (x - x_0)(x - x_n)$, then Eq. (2) is always true for any $\delta \ge 0$. Therefore, Eq. (2) does not control the magnitude of the shape modification. To control the magnitude of the shape modification indirectly, we add two additional constraints on the second derivative $\Delta r''(x)$ of $\Delta r(x)$ for smoothness control:

$$-\delta \le \Delta r''(x_0) \le \delta \quad \text{and} \quad -\delta \le \Delta r''(x_n) \le \delta \tag{3}$$

Then, constraints (2) and (3) with $\delta = 0$ will force $\Delta r(x) = 0$ because it is the only quadratic function that satisfies the conditions

$$\Delta r(x_0) = \Delta r(x_n) = \Delta r''(x_0) = \Delta r''(x_n) = 0$$

By using calculus and assuming that $l \ge 15$, one could prove that constraints (2) and (3) imply

$$|\Delta r(x)| \le 0.2 l^3 \delta \quad \text{for } 0 \le x \le l \tag{4}$$

That is, when δ is small, constraints (2) and (3) guarantee that $\Delta r(x)$ represents a small and smooth fuselage modification.

The smoothest shape modification strategy aims to achieve a given reduction rate of the objective function by using a shape modification $\Delta r(x)$ that minimizes the maximum value of $|\Delta r_i^{(3)}|$ $(0 \le i \le n)$, $|\Delta r''(x_0)|$, and $|\Delta r''(x_n)|$. This strategy forces smooth shape modifications and tries to keep modified configurations as close to the existing one as possible.

D. Fuselage Shape Optimization for Boom Minimization

Let $A_{e,i}$ be the total equivalent area of the configuration at $x_{e,i}$, where $0 = x_{e,0} < x_{e,1} < \ldots < x_{e,m} = l_e$ are the given effective distances. The total equivalent area $A_{e,i}$ includes the equivalent area due to volume and the equivalent area due to lift. (See [23,24] for calculation of the equivalent area due to volume, and see Eq. (3) in [45] for calculation of the equivalent area due to lift.) Let $A_{e,i}^*$ be a target equivalent area at $x_{e,i}$ for low-boom design. The design variables are fuselage radii at a given set of x locations: $0 = x_0 < x_1 < \ldots < x_n = l$.

The inverse design optimization problem is to find a fuselage shape such that

$$G(r_1, \ldots, r_{n-1}) = \sum_{i=0}^{m} (A_{e,i} - A_{e,i}^*)^2$$

is minimized. Unfortunately, no fuselage shape may exist that matches the target area distribution exactly (i.e., the minimum value of G is not zero) or multiple fuselage shapes may exist that make G almost zero. The problem is that a smaller value of G does not make the corresponding ground signature closer to the target ground signature. Therefore, in the case of no exact match, the goal is to match the A_e distributions as closely as possible over the longest possible range starting at $x_e = 0$ (see, for example, Fig. 9 of [21] and Fig. 21 of [20]).

For convenience, we use a column vector $\mathbf{r}$ to denote the design variables $r_1, \ldots, r_{n-1}$ and a row vector $\partial G/\partial \mathbf{r}$ to denote the gradient vector of partial derivatives of G with respect to $r_1, \ldots, r_{n-1}$. Then, for any particular design vector $\mathbf{r}_k$, the linear term $L(\mathbf{r}_k, \Delta\mathbf{r})$ in the Taylor polynomial approximation of G at $\mathbf{r}_k$ can be expressed as

$$G(\mathbf{r}_k + \Delta\mathbf{r}) - G(\mathbf{r}_k) \approx L(\mathbf{r}_k, \Delta\mathbf{r}) = \left\langle \frac{\partial G}{\partial \mathbf{r}}(\mathbf{r}_k), \Delta\mathbf{r} \right\rangle \tag{5}$$

After tedious calculations, one could get algebraic formulas of G and $\partial G/\partial \mathbf{r}$.

Now we are ready to describe a scheme for the interactive inverse design optimization of the fuselage shape for low-boom supersonic concepts. This scheme, called BOSS, uses the smoothest shape modifications of the fuselage to make the equivalent area distribution

move toward the target distribution interactively via some simple control parameters.

Algorithm for Boom Optimization Using Smoothest Shape Modifications

1) *Smoothness of shape modifications:* Let $\mathbf{r}_0$ be the current design vector. Choose a smoothness control parameter s between 0 and 10, where $s = 10$ means the smoothest shape modifications are used and $s = 0$ means no smoothness control is used for shape modifications. The Appendix describes how the smoothness control parameter s is used to define the feasible set of design variables.
2) *Reduction of matching errors:* Inspect the differences between the equivalent area of the configuration and the target. Choose an interval of effective distances $0 \le x_{e,\text{start}} < x_{e,\text{end}} \le l_e$ and the intended reduction rate ρ $(0 < \rho \le 1)$ for the accumulated matching error $\hat{G}$ over the range $x_{e,\text{start}} \le x_e \le x_{e,\text{end}}$.
3) *Selection of active design variables:* Determine the largest interval $x_{\text{start}} \le x \le x_{\text{end}}$ such that the accumulated matching error outside of $x_{e,\text{start}} \le x_e \le x_{e,\text{end}}$ is independent of small changes of r_i whenever $x_i < x_{\text{start}}$ or $x_i > x_{\text{end}}$.
4) *Optimization iteration:* For the given smoothness control parameter s, use an appropriate combination of the smoothest shape modification scheme and a trust region scheme to modify the design variables r_i that correspond to $x_{\text{start}} \le x_i \le x_{\text{end}}$ for reduction of the total matching error G until no further reduction is possible or G is reduced by $\rho\hat{G}$.

One key idea for optimization iteration in BOSS is to couple the smoothness constraints (2) and (3) with the following trust region constraints:

$$-\lambda_s\delta \le \Delta r(x_i) \le \lambda_s\delta \quad \text{for } 1 \le i \le n-1 \tag{6}$$

The scaling parameter $\lambda_s > 0$ is determined by s such that, if $s = 10$, the constraints (6) are automatically satisfied whenever Eqs. (2) and (3) hold; if $s = 0$, the constraints (2) and (3) are automatically satisfied whenever Eq. (6) holds; in general, the value of λ_s aims to maintain the ratio of the number of active constraints in Eqs. (2) and (3) vs the total number of active constraints as close as possible to $s/10$. It is a heuristic rule to transition from the smoothest shape modification scheme to a standard trust region scheme. The exact calculation of λ_s is given in the Appendix.

The selection of active design variables means no change of inactive design variables:

$$\Delta r(x_i) = 0 \quad \text{for } x_i < x_{\text{start}} \text{ or } x_i > x_{\text{end}} \tag{7}$$

The optimization iteration process is to solve a sequence of subproblems that minimize the linear approximation $L(\mathbf{r}_k, \Delta\mathbf{r})$ under constraints in Eqs. (2), (3), (6), and (7). However, instead of using numerical convergence rules, we use an objective function reduction rule to control the iterations.

The waiting time for a BOSS solution is indirectly controlled by users via two easy-to-understand control parameters: ρ and s. Obviously, if ρ is smaller, then the goal of the reduction of the objective function by $\rho\hat{G}$ is easier to achieve; moreover, if less restriction is imposed on the smoothness of $\Delta r(x)$ (i.e., a smaller value of s is used), then the reduction goal is also easier to achieve. A maximum waiting time of about 3 min is also implemented by setting a default value of 200 for the maximum number of iterations. As a result, BOSS terminates quickly with either a desirable solution or the best solution possible. This implementation allows a user to experiment with various choices of $x_{e,\text{start}}$, $x_{e,\text{end}}$, ρ, and s to close the gap interactively between the configuration's area distribution and the target. If an optimization iteration fails to find a desirable solution, then either no further improvement could be made in the specified range or any further reduction of G may require the use of less smooth fuselage shapes. The main usage of ρ is to reduce potential derivative bumps near the end points x_{start} and x_{end} of the active design variables. The smoothness constraints in Eq. (2) usually do not allow derivative bumps near the end points x_{start} and x_{end} in each iteration. However, a large value of $\rho\hat{G}$ might require many tiny derivative bumps to be accumulated during the iterations. If this happens, then one could use a reduced value of ρ and run BOSS several times with different values of $x_{e,\text{start}}$ and $x_{e,\text{end}}$ sequentially to achieve the desired reduction of G while avoiding any accumulation of derivative bumps. (See the Appendix for details of the optimization iteration in BOSS.)

VI. Case Study of Low-Boom Supersonic Conceptual Design

To demonstrate how BOSS can assist conceptual designers design low-boom supersonic concepts, in the following subsections, we document a design process for developing a low-boom supersonic concept from a low-drag supersonic concept.

A. Configuration Layout Design

A previously designed business jet configuration, shown in Fig. 8, was used as a starting point to develop a low-boom configuration. No consideration was given to the boom signature when this configuration was developed. It was developed to achieve the best performance, expressed as maximum range, for a given takeoff gross weight of 100,000 lb and a balanced field length of 7000 ft. The cabin was to be equivalent to that of a Citation X and the cruise Mach number was 1.8. This configuration was designed at the conceptual level to satisfy all of the practical considerations of the various disciplines, such as aerodynamics, structures, systems, low-speed performance, stability and control, and landing gear placement.

The wing planform was designed to achieve good supersonic cruise performance while maintaining adequate low-speed performance for takeoff and landing. Many studies done in conjunction with the High-Speed Research Program and earlier supersonic transport studies have shown that a cranked arrow-type planform is the preferred wing planform for most supersonic cruise missions that have a significant range requirement. The high leading-edge sweep angles of the inboard portion of the wing yield a low normal leading-edge Mach number and an adequate lifting length for drag minimization at cruise. The size and leading-edge sweep of the outboard panels were selected to minimize induced drag and maintain adequate low-speed performance for takeoff and landing with a minimum impact on the supersonic cruise performance.

Previous studies regarding leading-edge flaps on the inboard portion of the wing have shown an insensitivity to the leading-edge camber because of the low normal Mach number on these highly swept sections. Instead, improving the low-speed performance by increasing the leading-edge radius is more effective than using leading-edge flaps, which add weight and complexity to the wing. Leading-edge flaps on the outboard portion of the wing could have some aerodynamic benefit, but the challenge of integrating them into the thin outboard panel at this point appears to override any benefit. Trailing-edge flaps are used over the complete span because they can enhance the low-speed performance of the wing significantly. The trailing-edge flaps can also be used asymmetrically for roll control.

Aggressive use of fuselage area ruling was used to minimize wave drag. This was possible because the cabin area terminates just past the beginning of the main wing area. Fuel is carried in both the fuselage and wing. A significant portion of the fuel is carried in the fuselage aft of the cabin area. A T-tail arrangement is used for the vertical and horizontal tails, mainly to minimize the blocking of airflow over the tails by the wing at takeoff and landing angles of attack. The all-moving horizontal tail was sized for pitch control during takeoff and landing, and the vertical tail was sized using statistical data for engine-out conditions. The nacelles are located on the aft upper portion of the fuselage. This location is advantageous because it provides some noise shielding and alleviates the risk of foreign-object ingestion during takeoff and landing.

B. Low-Boom Design by Fuselage Shaping

For a given beginning-cruise weight of 96,500 lb, cruise altitude of 53,000 ft, cruise Mach of 1.8, an initial overpressure (0.5 psf), and

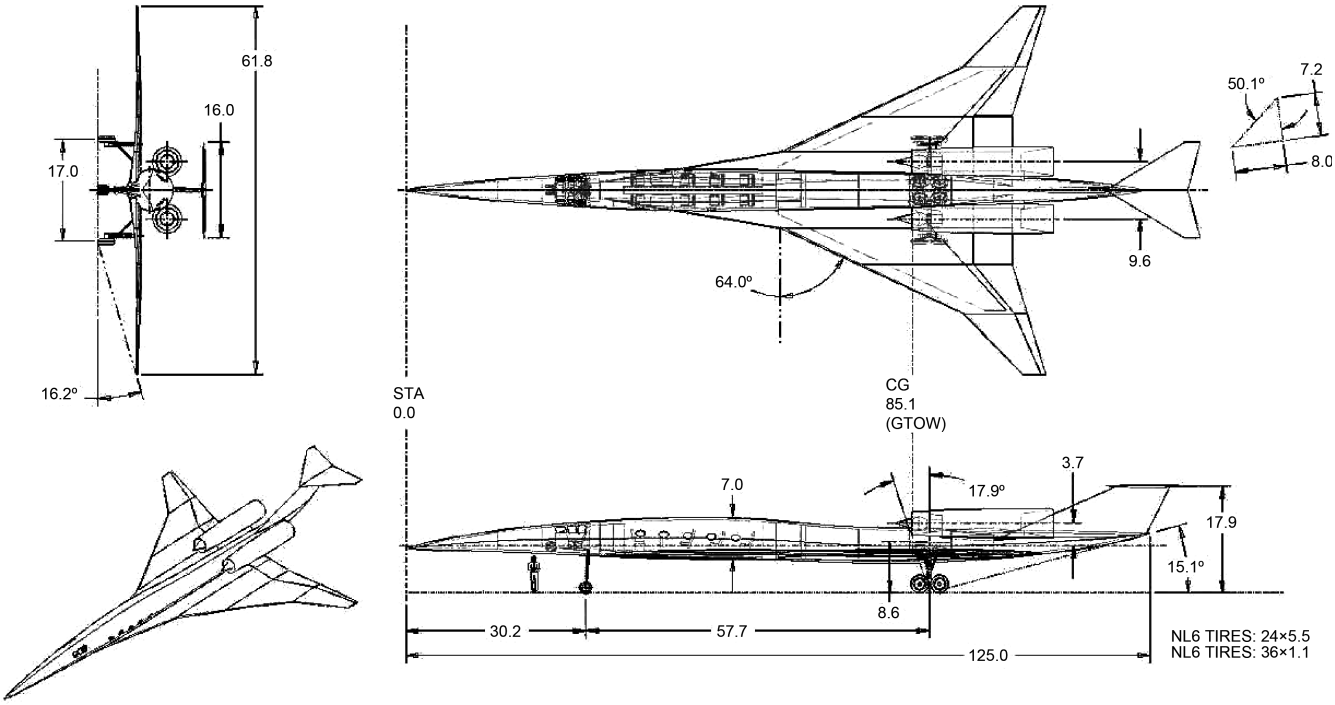

Fig. 8 Three-view of a supersonic business jet concept designed for performance.

two parameters defining the ground signature shape (the length of the flattop and the slope of the ramp), the ModelCenter model was used to generate a hybrid low-boom target signature and the corresponding A_e distribution. The boom signature and the total A_e distribution of the performance configuration were analyzed using the ModelCenter model and compared with the hybrid low-boom ground signature and the corresponding A_e distribution. Because no actual guidelines exist for defining an acceptable low-boom signature at this time, the hybrid signature is chosen as an acceptable target because it appears to allow for a more viable configuration than a flattop signature. The difficulty in using a flattop design is discussed later. The total A_e distribution that corresponds to this ground signature is calculated using the HYBRID code, which is also included in the ModelCenter model. Figure 9a illustrates the significant differences between the total equivalent areas for the performance configuration and the target. As stated in much of the literature that relates to low-boom design, the nose shape is critical to a shaped signature; therefore, the configuration area must match the target equivalent area closely near the nose. The other significant differences over the rest of the configuration can also have profound impact on the signature. The resulting boom signature is shown in Fig. 9b. Although not exactly an *N* wave, the peak of approximately 1.1 psf is only a few milliseconds after the initial overpressure, and the smallest differences in flight conditions will result in the typical *N* wave that is seen in virtually all supersonic configurations not designed specifically for a low-boom requirement.

The BOSS tool was used next to modify the fuselage areas to reduce the differences between the target and design equivalent areas. The BOSS tool allows significant flexibility in the way it can be used. In this case, the assumption was made that significant changes in the fuselage areas could be tolerated. The range over which BOSS was used was from 0 to 120 ft, in an effort to match the target equivalent area curve using almost the complete fuselage length. The smoothness control was set at fairly smooth ($s = 7$) and the reduction rate ρ was set at 55%. Figure 10a shows that, for approximately 60% of the effective distance range, a reasonable fit to the target can be accomplished. For the remaining portion of the effective distance range, the fuselage cross-sectional areas have decreased to near zero (see Fig. 11), but the corresponding equivalent areas do not match the target curve (see Fig. 10a). BOSS, therefore, quickly reveals that developing a feasible low-boom configuration by fuselage shaping alone would be extremely difficult. Furthermore,

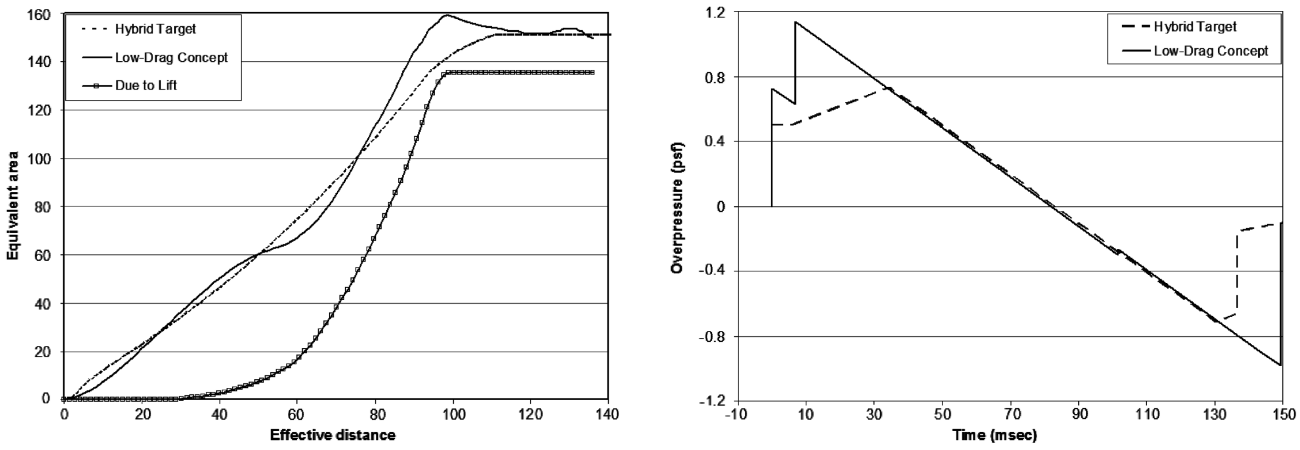

a) Comparison of equivalent areas **b) Comparison of ground signatures**

Fig. 9 Equivalent area distribution and ground signature of a low-drag supersonic concept.

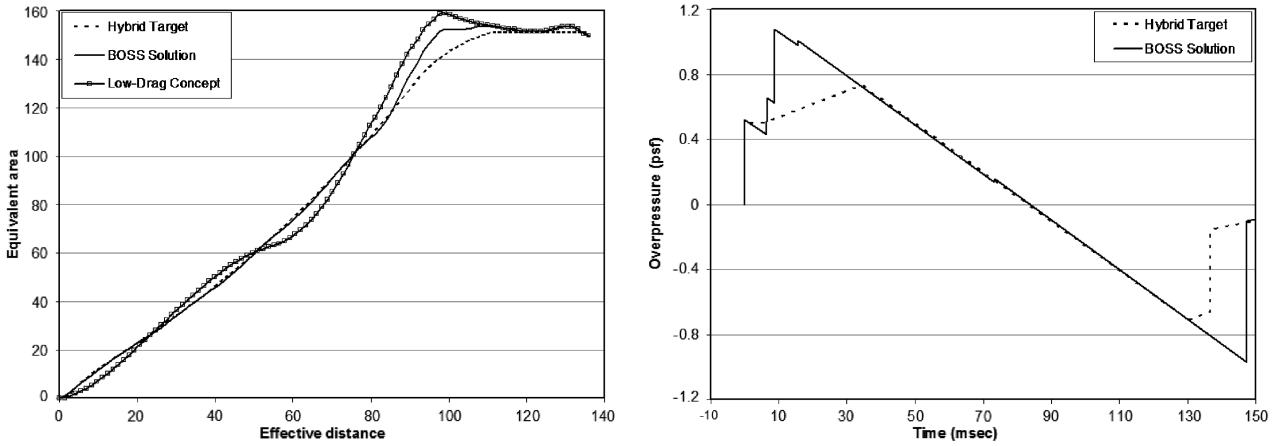

a) Comparison of equivalent areas b) Comparison of ground signatures

Fig. 10 Use of BOSS to obtain a low-boom concept by modifying the fuselage radii of the low-drag concept.

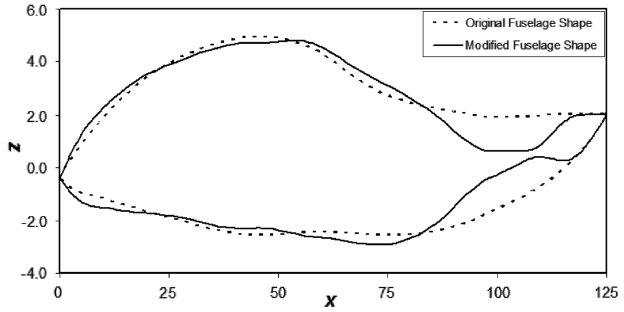

Fig. 11 Side view of the low-drag fuselage shape and the modified fuselage shape generated by BOSS.

Fig. 10b shows that the signature for such a configuration would not show any signature shaping benefit. This exercise also points out that a well-designed performance-based wing planform is probably not feasible for use on a low-boom configuration. Modifications to the planform are necessary to increase the lifting length of the configuration and distribute the lift of the configuration in a manner that allows for sufficient volume for the fuselage. Changes to the wing planform primarily include higher leading-edge sweep angles for all segments of the wing. These changes could actually enhance the cruise performance of the configuration if the optimum camber shape could be used, but this enhancement comes at the expense of low-speed performance, which is critical to takeoff and landing, and may result in a range penalty for the overall configuration.

The planform modifications are outside the scope of this paper but are nonetheless necessary to obtain a viable low-boom configuration. Some experience in low-boom supersonic configuration design is desirable to make these changes. The ModelCenter model includes a component called Planform Design, which allows some changes to be made easily to the original wing planform. This component was used in an iterative manner with both PBOOM and the signature calculation components to change the wing planform until enough volume could be included in the fuselage to develop a viable configuration. The fuselage was also lengthened by 5 ft so that more fuselage area was available to meet the target equivalent area curve and to make trimming and rotation easier. The ModelCenter model also includes a component called Component Processing for smoothing and changing fuselage shapes. Component Processing was used to modify the fuselage camber to more closely follow the camber shape of the inboard portion of the low-boom wing.

After these modifications are completed, the BOSS component is used to modify the fuselage radii for quick closure to a configuration that has a smooth fuselage shape with an acceptable low-boom ground signature. Because significant differences exist between the current A_e distribution and the target, in the first pass through BOSS, the range over which modifications could be made is set from $x_{e,\text{start}} = 0$ to $x_{e,\text{end}} = 120$ ft, the reduction rate ρ is set high at 80%, and the criteria for smoothness was set at fairly smooth shape ($s = 7$). These settings allow the fuselage area distribution to rapidly approach the target over a significant portion of the effective distance range. The results are fed back into the Component Processing program, where smoothing and changes to the fuselage camber line or area distribution can be made. In the second pass through BOSS, fitting is done on only the first 20 ft of the configuration because the nose shape is critical to shaping the signature. This process of fitting the area distribution to the target using BOSS and then changing and smoothing the fuselage shape with Component Processing is usually done several times until the fuselage area distribution and resulting boom signature are acceptable. Modifying the fuselage radii to match a target A_e distribution has in the past been one of the more time-consuming tasks in the low-boom supersonic conceptual design process. BOSS not only accomplishes this task much faster but also, when used in conjunction with the smoothing capability in the Component Processing program, allows for a fuselage area distribution that can be smooth in the second derivative. This is a feature that is highly desirable when attempting to achieve an acceptable low-boom signature. Figure 12 shows the final low-boom configuration. Although the resulting ground signature resembles the target signature pattern (see Fig. 13b), the differences between the A_e distributions are quite visible after $x_e = 50$ ft (see Fig. 13a).

The final A_e distribution in Fig. 13a is a low-boom area distribution derived by a designer, via a trial-and-error approach using planform modifications and fuselage shaping in succession, to best match the "unmatchable" target area distribution. This process usually takes several days to complete. A more desirable but unavailable method is to generate a target area distribution for a low-boom ground signature that is known a priori to be realizable by a credible supersonic concept with nacelles and tails.

Note that BOSS can be used to shape the fuselage for an almost perfect match of the equivalent areas. As an illustration, we run BOSS seven times with $x_{e,\text{start}} = 0$, $x_{e,\text{end}} = 130$ ft, and the reduction rate $\rho = 30\%$ after obtaining the low-boom fuselage. The resulting numerically optimum fuselage is shown in Fig. 14, with the corresponding area distribution and signature plotted in Figs. 15a and 15b, respectively. The smoothness control parameter s for each BOSS run is set to the highest value, from among 2, 3, 4, and 5, which allows a successful termination of BOSS. From the secondary axis in Fig. 15a, one can see that the absolute difference between the equivalent area of the numerically optimum concept and the target is less than 0.1 up to $x_e = 100$ ft. However, Fig. 14 shows that the numerically optimum fuselage shape is oscillatory and cannot be considered as a credible design. Thus, BOSS is capable of providing a numerically optimum solution to the inverse design problem in most cases, but the difficult part is finding a nearly optimal solution that can be considered as a credible conceptual design.

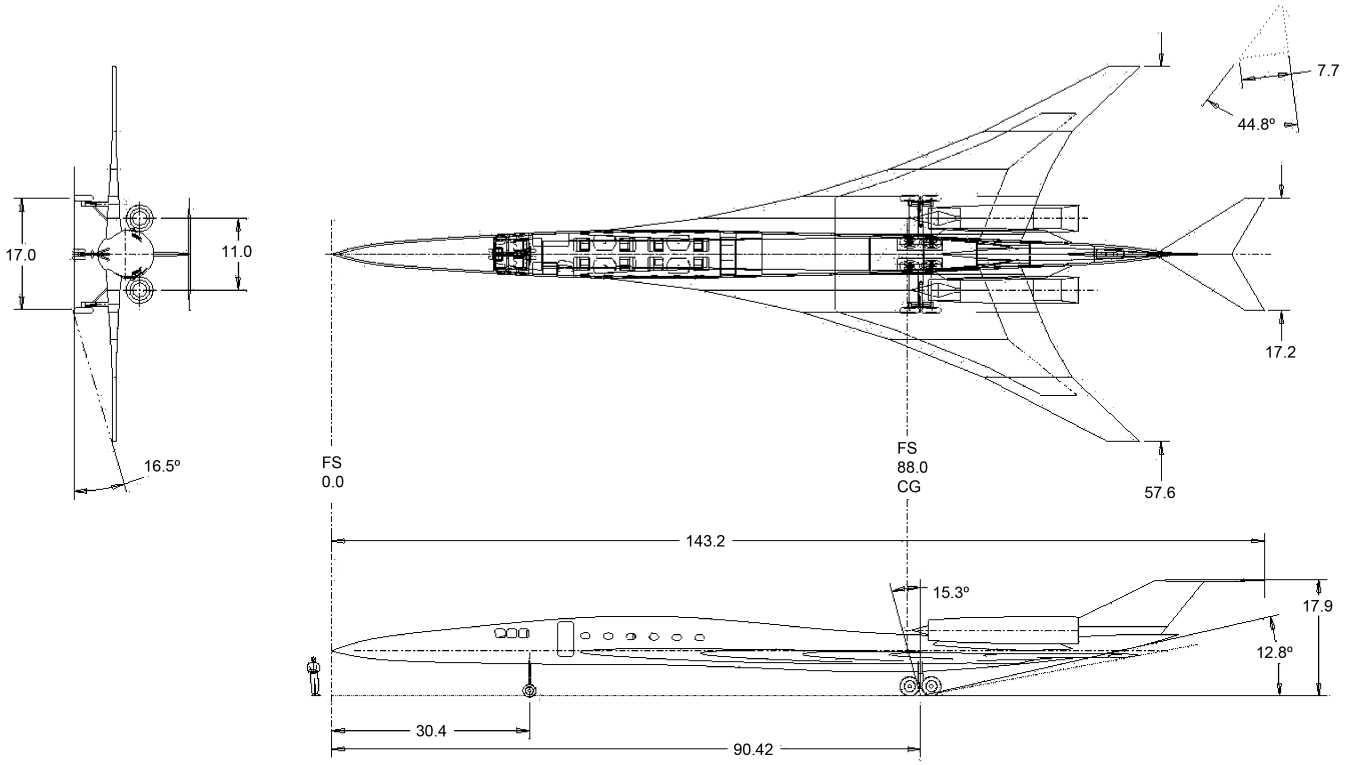

Fig. 12 Three-view of a low-boom supersonic business jet concept.

C. Trades Between Low-Boom and Aerodynamic Efficiency

The decision to not further reduce the differences between the two A_e distributions shown in Fig. 13a was also influenced by aerodynamic performance considerations. Adding additional area to the aft body of the fuselage was beginning to produce significant increases in the wave drag. A closer match in this area was not necessary to attain the initial overpressure desired, and any further wave drag increase would have an appreciable adverse effect on the performance of the configuration. It was decided that the configuration without the additional area was the best compromise between an acceptable low-boom signature and the performance of the configuration, while still satisfying the other practical constraints that are deemed necessary. This type of tradeoff is difficult to balance in a rigorous manner when designing a low-boom supersonic configuration at the conceptual level. Efforts to use purely numerical optimization methods usually lead to dubious configurations as a result of the lack of meaningful mathematical definitions for some of the practical constraints used by designers.

Performance of the low-boom configuration was calculated based on an initial gross takeoff weight of 100,000 lb. Low-speed and high-speed polars were calculated using the modified linear methods WINGDES and AERO2S [46], and wave drag was calculated using AWAVE [40]. These data, along with the geometric properties of the configuration, were entered in the sizing and performance code FLOPS [47]. Sizing was handled by holding the gross takeoff weight at 100,000 lb, whereas thrust and wing area were the design variables. The primary constraints were takeoff and landing field length, with takeoff field length being the most critical. The modifications of the fuselage shape and wing planform to achieve a viable low-boom configuration decreased the low-speed aerodynamic performance; thus, the engine size had to increase to meet the takeoff constraint. To a lesser extent, the fuselage shaping for low boom also increased the wave drag, which had an adverse impact on the cruise portion of the mission. The overall impact of the changes that were made to create a viable low-boom configuration resulted in a decrease in range from 3500 to 3000 n mile, or about a 15% decrease in performance when

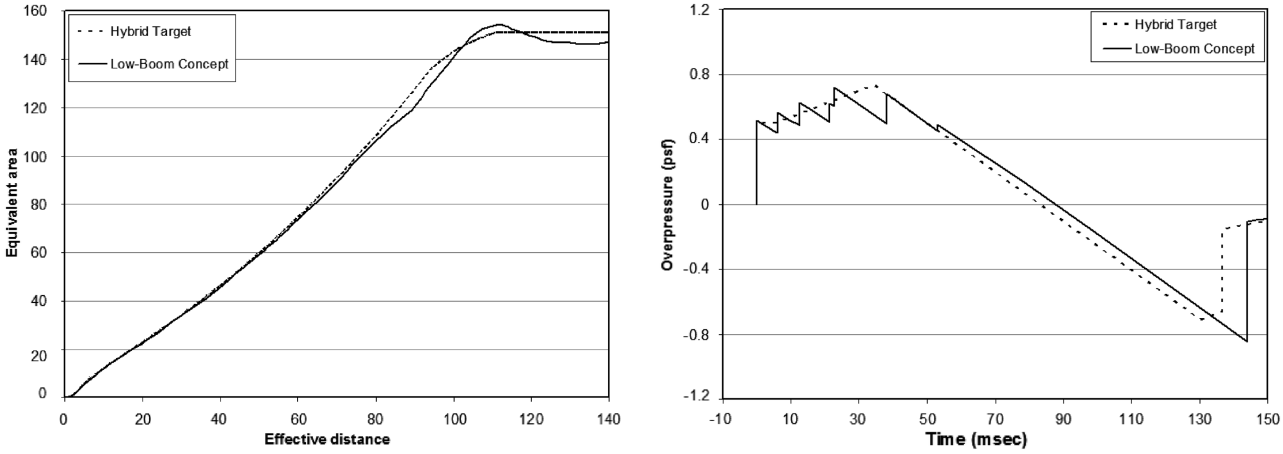

a) Comparison of equivalent areas **b) Comparison of ground signatures**

Fig. 13 Equivalent area distribution and ground signature of a low-boom concept.

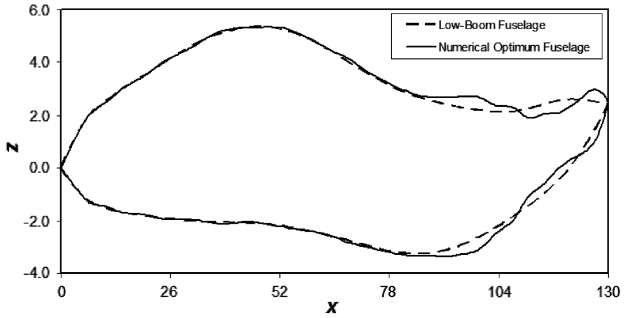

Fig. 14 Side view of low-boom fuselage and numerically optimum fuselage.

measured in this manner. A fruitful area for further design refinement is how to modify the configuration to minimize this penalty and maintain an acceptable low-boom signature.

D. Effects of Target Ground Signatures

After a viable low-boom configuration is obtained, studies can be completed quickly to determine how variations in the target signature would impact the configuration. One such variation would be to change our target signature from a hybrid to a flattop signature. Flattop signatures are less likely than the hybrid signatures to be degraded by changes in the atmosphere. The flattop target signature is generated by changing the slope parameter in the HYBRID code, which also calculates the corresponding total target A_e distribution. The fuselage of the configuration is then modified using BOSS to match the target A_e distribution, and the results are shown in Figs. 16a and 16b. Figure 16a shows that BOSS matched the target A_e distribution quite well, and Fig. 16b shows that the signature is indeed approaching a flattop shape with only a few BOSS runs. However, Fig. 17 shows that the fuselage cross-sectional areas in the aft portion of the fuselage decrease to the extent that obtaining a viable low-boom configuration by fuselage shaping alone would be difficult. Therefore, designing a supersonic concept with a flattop signature requires either further wing planform changes or lengthening of the fuselage or both. Because these types of studies can be done quickly, many such questions about how fundamental changes to the configuration affect the viability of the configuration and the impact they have on the signature can be addressed at the conceptual design level with little effort. It is important to answer as many of these questions as possible early in the design process before more time-consuming and expensive analyses and tests are performed.

VII. Relationship Between Area Distribution and Ground Signature

From the previous case study of low-boom conceptual design, it is clear that a target area distribution derived from the SGD theory may not be realized by a practical supersonic concept with nacelles and tails. The designer must find a configuration for which the A_e distribution closely matches the target in such a way that the resulting ground signature is similar to the target low-boom signature. The ground signature of the final low-boom concept may be similar to the target signature (see Fig. 13b), but the two A_e distributions are visibly different (see Fig. 13a). Even with almost perfect matching of A_e distributions, sawtooth oscillations still exist in the ground signature of the configuration (see Figs. 15a and 15b). These results show two characteristics of the relationship between the equivalent area distribution and the ground signature: 1) similarly shaped ground signatures can have significantly different A_e distributions, and 2) sawtooth oscillations in ground signatures are unavoidable for supersonic concepts with nacelles and tails. In this section, we attempt to provide some insight into these two characteristics of the relationship between the A_e distribution and the boom signature.

Let $\mathcal{E}$ be the envelope generated by the graphs of the A_e distributions corresponding to the ramp, hybrid 1, . . ., hybrid 4, and flattop signatures plotted in Fig. 1a. Then, the A_e distribution for the low-boom design lies in $\mathcal{E}$ for $x_e < 80$ ft (see Fig. 18). We can conjecture that other A_e distributions can be found in the envelope region $\mathcal{E}$ with low-boom ground signature. No general method exists to define a target A_e distribution in $\mathcal{E}$ with a low-boom ground signature. However, one can easily construct low-boom A_e distributions that are different from those derived by the SGD theory.

Let $A_{e,1}(x_e)$ and $A_{e,2}(x_e)$ be two A_e distributions that correspond to the low-boom signatures plotted in Fig. 1a. Then, the following convex combination $A_e^*(x_e)$ of these two A_e distributions also has a low-boom ground signature

$$A_e^*(x_e) = \tau(x_e)A_{e,1}(x_e) + [1 - \tau(x_e)]A_{e,2}(x_e) \tag{8}$$

where $\tau(x_e)$ is a linear polynomial with its values between zero and one for $0 \le x_e \le l_e$. Figure 19a shows how the three constructed A_e distributions differ from the A_e distribution for the hybrid 2 (H2) signature, where HiHj denotes a convex combination of hybrid i and hybrid j. These constructed A_e distributions have the same characteristics as the original hybrid signatures (see Fig. 19b).

The need for a new target A_e distribution usually arises when the given target becomes incompatible with the volume requirement for a practical configuration. For low-boom supersonic concept design using Whitham's boom prediction method [4,5], it is important to have a capability to increase or decrease the value of a given A_e target over a specific x_e range without adverse effect on the predicted ground signature. Methods that are more flexible than using convex combinations of A_e distributions derived by the SGD theory need to be developed.

In Whitham's boom prediction theory, each vertical line segment in the boom signature is caused by shock waves. However, we do not yet understand how numerical errors in the calculation of the A_e distribution affect the oscillations in the predicted ground signature.

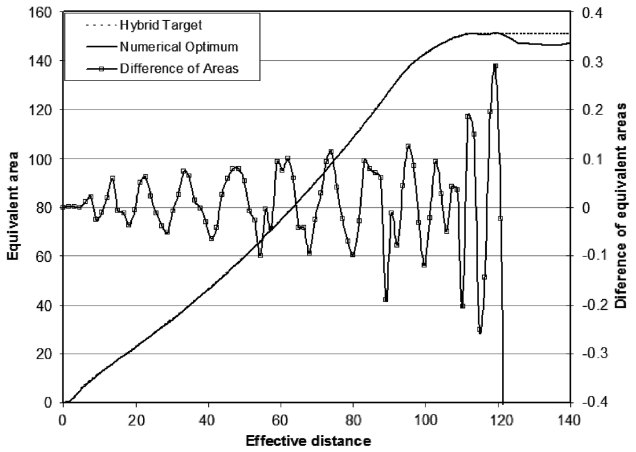

a) Comparison of equivalent areas

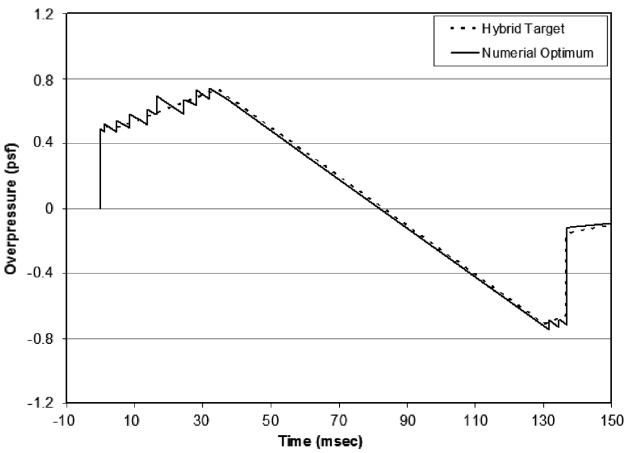

b) Comparison of ground signatures

Fig. 15 Equivalent area distribution and ground signature of a numerically optimum concept.

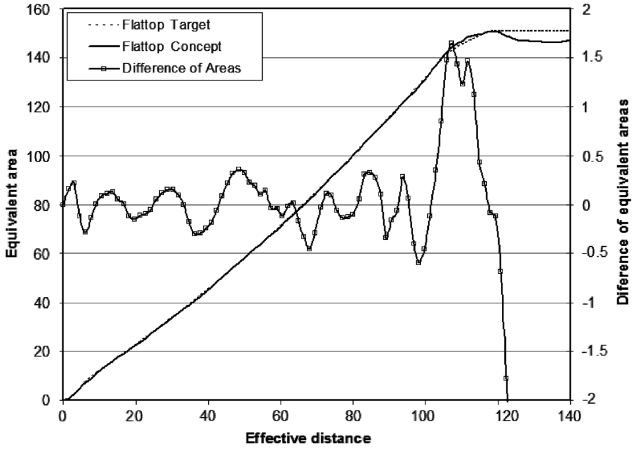

a) Comparison of equivalent areas

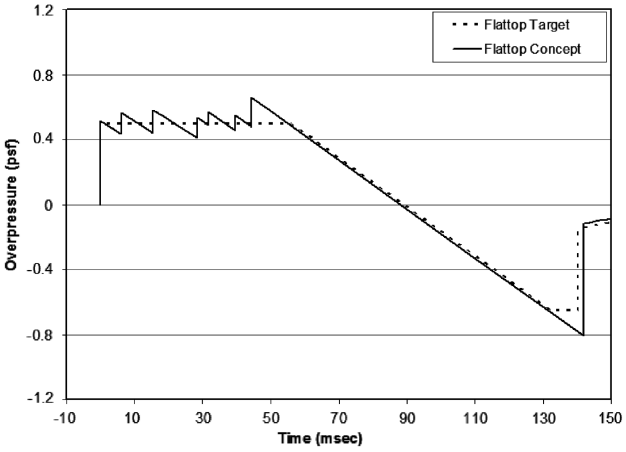

b) Comparison of signatures

Fig. 16 Ground signature and area distribution of a flattop supersonic concept.

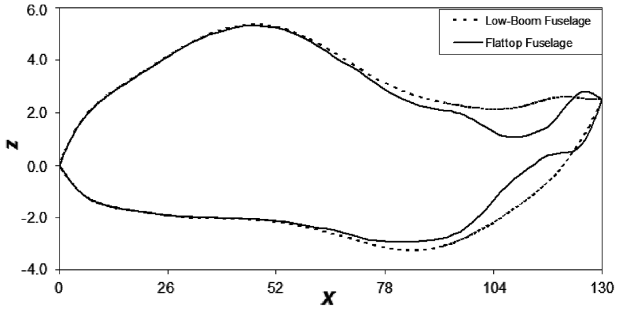

Fig. 17 Side view of the fuselage for the flattop concept.

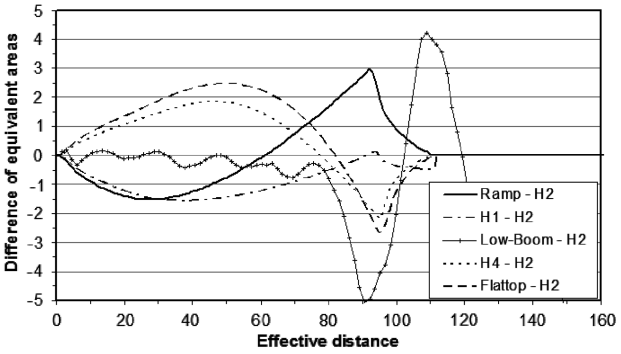

Fig. 18 Deviations of other equivalent area distributions from that for hybrid 2.

Note that the differences between the A_e distribution for the low-boom design and the target are caused by both the numerical errors in the A_e calculation and the actual mismatch of the A_e distributions. Numerical errors in the A_e calculation include numerical errors in the lift distribution and discretization errors in the design's volume calculation. These two sources of errors cannot be separated. Therefore, we can only assess their cumulative effect on the ground signature. The basic method is to eliminate the matching errors over various x_e ranges to see how the predicted ground signature changes. The process is to use a convex combination $A^*(x_e)$ of $A_e(x_e)$ of the low-boom design and the target $A_{e,\text{target}}$ defined by the following formula:

$$A_e^*(x_e) = \tau(x_e)A_e(x_e) + [1 - \tau(x_e)]A_{e,\text{target}}(x_e) \tag{9}$$

where $\tau(x_e)$ is a piecewise linear polynomial defined by one of the following two formulas:

$$\tau(x_e) = \begin{cases} 0 & \text{if } x_e \le x_e^* \\ \frac{x_e - x_e^*}{l_e - x_e^*} & \text{if } x_e > x_e^* \end{cases} \quad \text{or} \quad \tau(x_e) = \begin{cases} 0 & \text{if } x_e > x_e^* \\ \frac{x_e^* - x_e}{x_e^*} & \text{if } x_e \le x_e^* \end{cases} \tag{10}$$

Figure 20a shows the differences of $A_e^*(x_e)$ generated by the first formula in Eq. (10) and the target distribution, with $x_e^* = 10, 40, 70,$ and 100. Figure 20b shows how the oscillations in the front part of the predicted ground signature gradually disappear as the matching errors become zero for $x_e \le x_e^*$ (=10, 40, 70, and 100). Figure 21a shows the differences of $A_e^*(x_e)$ generated by the second formula in Eq. (10) and the target distribution, with $x_e^* = 90, 70, 40,$ and 10. Figure 21b shows that the aft part of the predicted ground signature

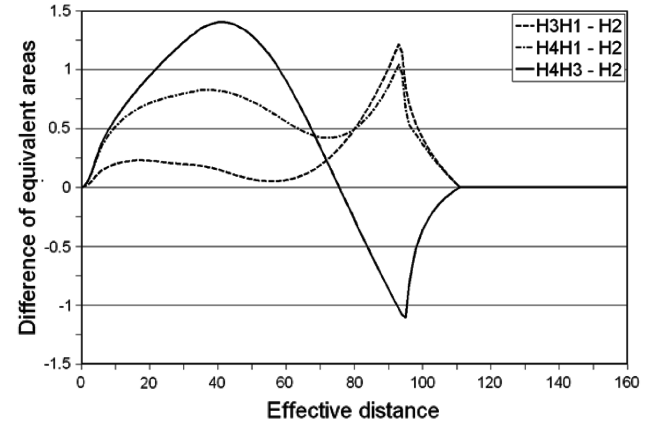

a) Comparison of equivalent areas

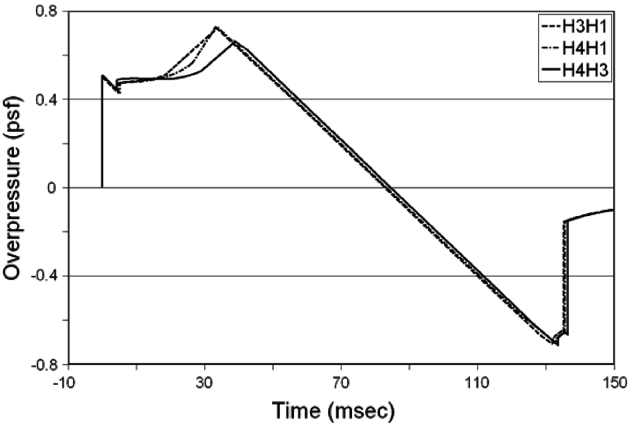

b) Comparison of signatures

Fig. 19 Ground signature and area distribution of a flattop supersonic concept.

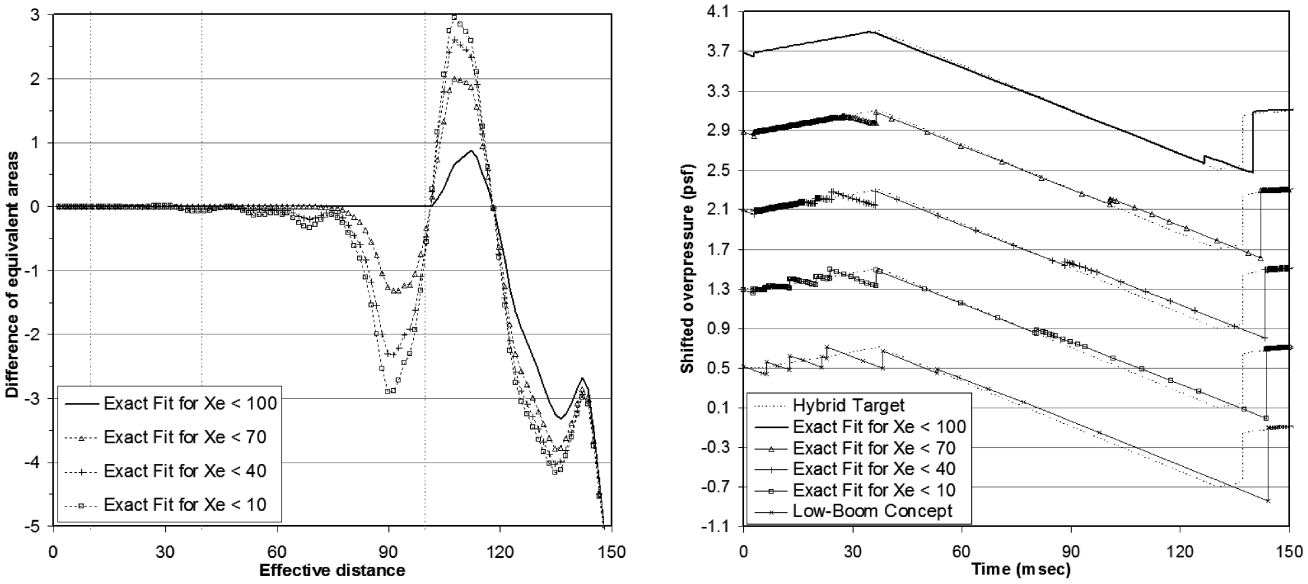

a) Comparison of matching errors **b) Comparison of signatures**

Fig. 20 Sensitivity of predicted ground signatures with respect to aft A_e matching errors.

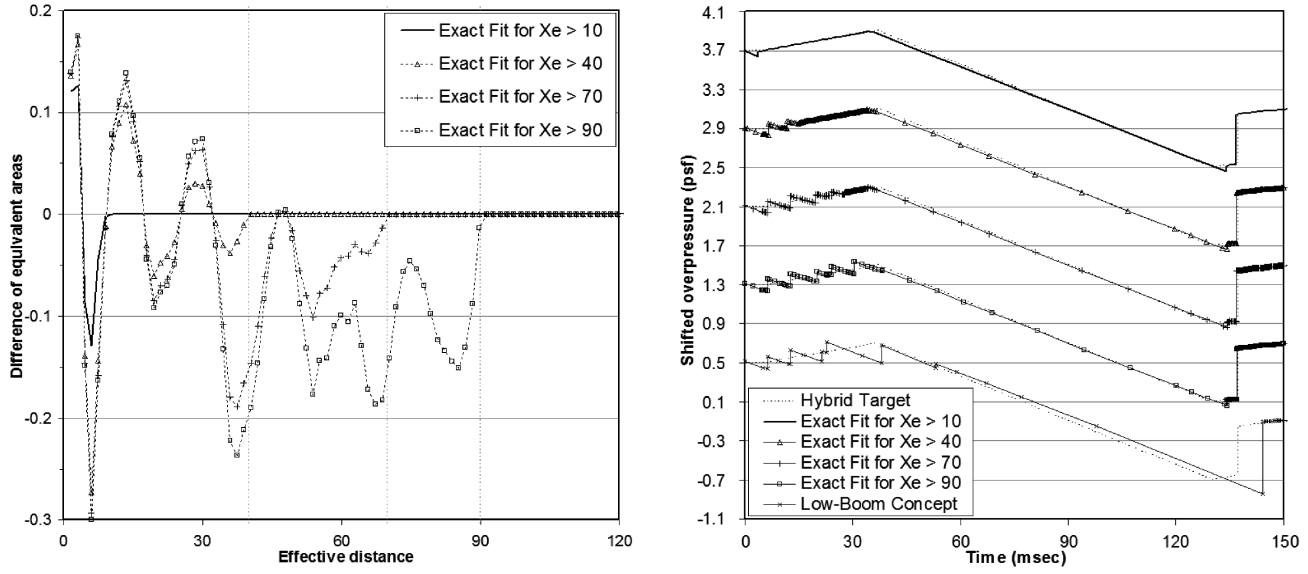

a) Comparison of matching errors **b) Comparison of signatures**

Fig. 21 Sensitivity of predicted ground signatures with respect to front A_e matching errors.

matches the target signature when the matching errors become zero for $x_e \geq 90$, and it also shows how the oscillations in the front part of the predicted ground signature gradually disappear as the matching errors become zero for $x_e \geq x_e^*$ (=90, 70, 40, and 10). In practice, achieving the perfect matching of A_e distributions over any reasonable range of x_e is impossible. As a result, the predicted ground signature will always contain oscillations because of its sensitivity with respect to the second derivative of the A_e distribution.

VIII. Conclusions

In this paper, we introduce an interactive design optimization tool called BOSS (boom optimization using smoothest shape modifications), for generating low-boom configurations by modifying the fuselage shape to reduce the discrepancies between the design A_e distribution of a supersonic concept and a target distribution derived from the boom minimization theory.

The boom prediction code based on Whitham's F-function method, PBOOM, is used for sonic-boom analysis [4,5]. BOSS uses the smoothest shape modification strategy to modify the fuselage radius distribution at 100 or more longitudinal locations and to find smooth fuselage shapes that reduce the discrepancies between the design and target A_e distributions over any specified range of effective distance. A smoothing tool is also incorporated into the design process so that any minor oscillation in the resultant fuselage radius distribution can be easily removed with minimum change to the fuselage shape. All the tools are integrated as plug-and-play components in the ModelCenter framework.

For any given supersonic concept (with wing, fuselage, nacelles, tails, and optional canards), a designer can examine the differences between the design and target equivalent areas, decide which part of the design equivalent area curve needs to be modified, choose a desirable rate for the reduction of the discrepancies over the specified range, and select a parameter for smoothness control of fuselage shapes. Then BOSS generates a fuselage shape based on the designer's inputs in a matter of seconds. If the generated solution is not acceptable, the designer can work on a different part of the equivalent area curve, change the rate of reduction, or relax the

smoothness control until a desirable solution is found. The new configuration is analyzed by PBOOM to determine whether it has an acceptable low-boom ground signature. If not, the designer can use BOSS to further reduce the differences between the design and target equivalent areas until the configuration has an acceptable low-boom ground signature. Using BOSS and PBOOM, the designer can generate a realistic, smooth fuselage shape that results in a supersonic configuration with a low-boom ground signature in a few hours. In addition, a designer can use BOSS to quickly eliminate any configuration that cannot achieve low-boom characteristics with fuselage shaping alone.

For any given wing planform and layout of aircraft components, BOSS reduces the design time of low-boom supersonic concepts from months to hours. More important, BOSS allows a quick closure of the fuselage shaping process because BOSS lets the designer see how much deterioration of the fuselage shape is necessary for further reduction of the discrepancies between the design and target A_e distributions.

A conceptual design case study demonstrates how BOSS can be used to develop a low-boom supersonic concept from a low-drag supersonic concept.

The perturbation study demonstrates that oscillations in the sonic-boom signature may be unavoidable because exact matching of the target A_e distribution is unlikely. In addition, the study also shows that making the target A_e distributions realizable by a practical configuration, while maintaining a shaped sonic-boom signature, is desirable. One approach to generating alternate A_e distributions is demonstrated by using convex combinations of target A_e distributions from the SGD theory. However, the question of whether these new A_e distributions could be matched by practical configurations has not been answered.

The next step is to integrate CFD analysis into the current low-boom conceptual design process to make the generated low-boom concept more credible. Also, BOSS can be extended to make it applicable to a fuselage with noncircular cross sections.

Appendix: Optimization Iterations in BOSS

1) *Range of* λ_s. Each constraint in Eqs. (2) and (3) can be expressed as

$$-\delta \le \sum_{j=1}^{n-1} \kappa_j \Delta r_j \le \delta$$

where κ_j are coefficients for the linear combination. Let $\lambda_{\min}$ be the reciprocal of the maximum value of

$$\sum_{j=1}^{n-1} |\kappa_j|$$

and $\lambda_{\max} = 0.2l^3$. Then, the constraints in Eqs. (2) and (3) are automatically satisfied if Eq. (6) holds for $\lambda_s = \lambda_{\min}$. On the other hand, the constraints in Eq. (6) are automatically satisfied for $\lambda_s = \lambda_{\max}$ if Eqs. (2) and (3) hold.

2) *Values of* λ_s *for* $s = 0$ or 10. Set $\lambda_s = \lambda_{\min}$ (i.e., no smoothness constraint is used) if $s = 0$, and set $\lambda_s = \lambda_{\max}$ (i.e., the feasible solutions are completely determined by the smoothness constraints) if $s = 10$.

3) *Estimation of* λ_s *for* $0 < s < 10$. Let $\lambda_s = 1$. Find $\delta > 0$ such that the minimum value of $L(\mathbf{r}_0, \Delta\mathbf{r})$ is $-\rho\hat{G}$ under the constraints in Eqs. (2), (3), (6), and (7), where

$$\hat{G} = \sum_{x_{e,\text{start}} \le x_{e,i} \le x_{e,\text{end}}} (A_{e,i} - A^*_{e,i})^2$$

Then, fix δ and find $\lambda_s > 0$ such that the ratio of the number of active constraints in Eqs. (2) and (3) to the total number of active constraints in Eqs. (2), (3), and (6) is approximately $s/10$.

4) *Initial Reduction.* Assume that a total reduction of $\rho\hat{G}$ could be achieved in 100 iterations. Set $\rho_0 = \rho\hat{G}/100$ and $k = 0$.

5) *Iteration for Trusted Reduction.* Find $\delta > 0$ such that the minimum value of $L(\mathbf{r}_k, \Delta\mathbf{r})$ is $-\rho_k$ under the constraints in Eqs. (2), (3), (6), and (7). Let $\Delta\mathbf{r}_k$ be the solution of the following strictly convex quadratic programming problem:

$$\min_{\Delta\mathbf{r}} L(\mathbf{r}_k, \Delta\mathbf{r}) + 10^{-9} \sum_{i=1}^{n-1} \Delta r(x_i)^2 \tag{A1}$$

subject to the constraints in Eqs. (2), (3), (6), and (7).

6) *Update the Solution.* Set $\mathbf{r}_{k+1} = \mathbf{r}_k + \Delta\mathbf{r}_k$.

7) *Check for Termination.* If $G(\mathbf{r}_{k+1}) \le G(\mathbf{r}_0) - \rho\hat{G}$, then output $\mathbf{r}_{k+1}$ as the solution and terminate the iteration.

8) *Reject the Update if Necessary.* If $G(\mathbf{r}_k) - G(\mathbf{r}_{k+1}) \le 0$, then reset $\mathbf{r}_{k+1} = \mathbf{r}_k$.

9) *Adjust Reduction Rate if Necessary.* If $G(\mathbf{r}_k) - G(\mathbf{r}_{k+1}) > 0.85\rho_k$, then $\rho_{k+1} = 2\rho_k$; if $G(\mathbf{r}_k) - G(\mathbf{r}_{k+1}) < 0.35\rho_k$, then $\rho_{k+1} = \rho_k/2$; otherwise, $\rho_{k+1} = \rho_k$. If $k < 200$, then go back to step 5; otherwise, output $\mathbf{r}_{k+1}$ as the solution and terminate the iteration.

Note that iteration control parameters, such as ρ_0, the updating formulas for ρ_k, and the maximum number (200) of iterations, in BOSS are set heuristically based on some preliminary numerical tests. One can use other equally plausible choices. The maximum number of iterations is chosen to achieve a maximum waiting time of 3 min for each BOSS run.

For an inequality constraint $C_{\min} \le C(\Delta\mathbf{r}) \le C_{\max}$, the constraint is active for an optimal solution $\Delta\mathbf{r}$ if either $C(\Delta\mathbf{r}) = C_{\min}$ or $C(\Delta\mathbf{r}) = C_{\max}$. For example, $-\lambda_s\delta \le \Delta\mathbf{r}(x_i) \le \lambda_s\delta$ is called an active constraint if either $\Delta r(x_i) = -\lambda_s\delta$ or $\Delta r(x_i) = \lambda_s\delta$. The scale λ_s is a heuristic rule to control the smoothness of shape modifications $\Delta\mathbf{r}$. The number of active constraints in Eq. (6) implicitly determines how much more influence Eq. (6) has on the optimal solution than Eqs. (2) and (3). By changing the value of λ_s, we implicitly control the potential influence Eq. (6) has on the optimal solution (i.e., the roughness of the shape modification).

Equation (A1) is based on Mangasarian's theory on the least norm solution of a linear program [48]. In theory, one should replace 10^{-9} by a sufficiently small positive number to guarantee that the solution of Eq. (A1) is actually a minimizer of $L(\mathbf{r}_k, \Delta\mathbf{r})$ under the same set of constraints. But 10^{-9} works very well in our numerical experiments. In the case without smoothness constraints, Eq. (A1) forces the optimal solution to stay as close to $\mathbf{r}_k$ as possible while achieving the same reduction of the linear approximation $L(\mathbf{r}_k, \Delta\mathbf{r})$ of the objective function G.

Steps 3 and 5 involve solutions of several linear programming problems of less than 200 variables, each of which can be solved in a fraction of seconds. For any given δ, let $L^*_k(\delta)$ be the minimum value of $L(\mathbf{r}_k, \Delta\mathbf{r})$ under the constraints in Eqs. (2), (3), (6), and (7). Then, $L^*_k(\delta)$ is a decreasing function of δ with $L^*_k(0) = 0$. For any given negative target value $L_{\text{target}} < 0$, exactly one value of $\delta > 0$ exists such that $L^*_k(\delta) = L_{\text{target}}$. This equation can be efficiently solved by many known methods because of the monotonicity of $L^*_k(\delta)$. We use a standard root-finding method that uses linear rational function predictions.

Root-Finding Method Using Linear Rational Function Predictions:

1) *Initialization.* Set $\delta_0 = 0$ and $\delta_1 = 1$. Compute $L^*_k(1)$. Set $\delta_2 = L_{\text{target}}/L^*_k(1)$. Compute $L^*_k(\delta_2)$.

2) *Linear Rational Function Interpolation.* Let $\eta(t) = (t + c_0)/(c_1 t + c_2)$ be the interpolant of three data points $(\delta_0, L^*_k(\delta_0))$, $(\delta_1, L^*_k(\delta_1))$, and $(\delta_2, L^*_k(\delta_2))$. That is, $\eta(\delta_i) = L^*_k(\delta_i)$ for $0 \le i \le 2$.

3) *Linear Rational Function Prediction.* Find $\delta > 0$ such that $\eta(\delta) = L_{\text{target}}$ and compute $L^*_k(\delta)$.

4) *Check for Termination.* If $|L^*_k(\delta) - L_{\text{target}}|/|L_{\text{target}}| < 0.00001$ or a maximum number (40) of iterations is reached, then output δ as the solution.

5) *Update for Next Iteration.* Let j be the index such that δ_j is the farthest away from δ among δ_0, δ_1, and δ_2. Replace δ_j by δ. Go back to step 2.

The preceding root-finding algorithm usually terminates after solving 3–15 linear programming problems because the linear rational function provides an excellent approximation of the nonlinear behavior of $L_k^*(\delta)$. This algorithm is used in step 5 of the optimization iterations for BOSS so that the total cost of each iteration in BOSS is approximately that of solving 4–16 linear or quadratic programming problems. For $n = 120$, each iteration in BOSS usually takes less than 1 s when executed on a typical UNIX computer server.

Replacing δ and $L_k^*(\delta)$ with λ_s and the ratio of the number of active constraints in Eqs. (2) and (3) to the total number of active constraints, respectively, we can apply the preceding root-finding method to find λ_s in step 2 of optimization iterations in BOSS. In this case, we allow the maximum number of iterations to be 80 instead because the value of λ_s is only estimated once. The average waiting time for BOSS is usually less than 30 s when $n = 120$.

References

[1] Seebass, R., and George, A., "Sonic-Boom Minimization," *Journal of the Acoustical Society of America*, Vol. 51, No. 2, Pt. 3, 1972, pp. 686–694. doi:10.1121/1.1912902

[2] Darden, C., "Minimization of Sonic Boom Parameters in Real and Isothermal Atmosphere," NASA TN-D-7842, 1975.

[3] Darden, C., "Sonic Boom Minimization with Nose-Bluntness Relaxation," NASA TP-1348, 1979.

[4] Whitham, G., "Flow Pattern of a Supersonic Projectile," *Communications on Pure and Applied Mathematics*, Vol. 5, No. 3, 1952, pp. 301–348. doi:10.1002/cpa.3160050305

[5] Walkden, F., "Shock Pattern of a Wing-Body Combination, Far from the Flight Path," *Aeronautical Quarterly*, Vol. 9, May 1958, pp. 164–194.

[6] McMasters, J., and Cummings, R., "Airplane Design: Past, Present, and Future," *Journal of Aircraft*, Vol. 39, No. 1, 2002, pp. 10–17.

[7] Seebass, R., and Argrow, B., "Sonic Boom Minimization Revisited," *The 2nd Theoretical Fluid Mechanics Meeting*, AIAA Paper 1998-2956, June 1998.

[8] Morgenstern, J., "Low Sonic Boom Design and Performance of a Mach 2.4/1.8 Overland High Speed Civil Transport," *High-Speed Research: Sonic Boom*, Vol. 2. edited by C. Darden, NASA CP-3173, Feb. 1992, pp. 55–63.

[9] Haglund, G., and Ogg, S., "Two HSCT Mach 1.7 Low Boom Designs," *High-Speed Research: Sonic Boom*, Vol. 2, edited by C. Darden, NASA, CP-3173, Feb. 1992, pp. 65–87.

[10] Makino, Y., Sugiura, T., Watanuki, T., Kubota, H., Aoyama, T., and Iwamiya, T., "Effect of Nose Bluntness of a Low-Boom Configuration on Sonic-Boom," *15th AIAA Applied Aerodynamics Conference*, AIAA Paper 1997-2213, June 1997.

[11] Makino, Y., Suzuki, K., Noguchi, M., and Yoshida, K., "Non-Axisymmetrical Fuselage Shape Modification for Drag Reduction of a Low Sonic-Boom Airplane," *41st Aerospace Sciences Meeting and Exhibit*, AIAA Paper 2003-557, Jan. 2003.

[12] Makino, Y., Suzuki, K., Noguchi, M., and Yoshida, K., "Nonaxisymmetrical Fuselage Shape Modification for Drag Reduction of Low-Sonic-Boom Airplane," *AIAA Journal*, Vol. 41, No. 8, 2003, pp. 1413–1420.

[13] Sasaki, D., and Obayashi, S., "Low-Boom Design Optimization for SST Canard-Wing-Fuselage Configuration," *16th AIAA Computational Fluid Dynamics Conference*, AIAA Paper 2003-3432, June 2003.

[14] Graham, D., Dahlin, J., Meredith, K., and Vadnais, J., "Aerodynamic Design of Shaped Sonic Boom Demonstration Aircraft," *43rd AIAA Aerospace Sciences Meeting and Exhibit*, AIAA Paper 2005-8, Jan. 2005.

[15] Haglund, G., "High Speed Civil Transport Design for Reduced Boom," Boeing Document No. D6-55430, NASA, Contract No. NAS1-18377, 1991.

[16] Mack, R., and Haglund, G., "Practical Low-Boom Overpressure Signature Based on Minimum Sonic Boom Theory," *High-Speed Research: Sonic Boom*, Vol. 2, edited by C. Darden, NASA, CP-3173, Feb. 1992, pp. 15–30.

[17] Mack, R., and Needleman, K., "Methodology for Designing Aircraft to Low Sonic Boom Constraints," NASA TM-4246, 1991.

[18] Mack, R., "Additional *F*-Functions Useful for Preliminary Design of Shaped-Signature, Low-Boom, Supersonic-Cruise Aircraft," NASA CP-209699, Dec. 1999.

[19] Shepard, K., and Sullivan, B., "Loudness Calculation Procedure Applied to Shaped Sonic Booms," NASA TP-3134, 1991.

[20] Aronstein, D., and Schueler, K., "Two Supersonic Business Aircraft Conceptual Designs with and Without Sonic Boom Constraint," *Journal of Aircraft*, Vol. 42, No. 3, 2005, pp. 775–786. doi:10.2514/1.7578

[21] Mack, R., "Supersonic Business-Jet Concept Designed for Low Sonic Boom," NASA TM-212435, 2003.

[22] Choi, S., Alonso, J., and Weide, E., "Numerical and Mesh Resolution Requirements for Accurate Sonic Boom Prediction of Complete Aircraft Configurations," *42nd AIAA Aerospace Sciences Meeting and Exhibit*, AIAA Paper 2004-1060, Jan. 2004.

[23] Barger, R., and Adams, M., "Fuselage Design for a Specified Mach-Sliced Area Distribution," NASA TP-2975, 1990.

[24] Mack, R., and Needleman, K., "Semiempirical Method for Obtaining Fuselage Normal Areas from Fuselage Mach Sliced Area," NASA TM-4228, 1990.

[25] Rallabhandi, S., and Mavris, D., "Sonic Boom Minimization Using Inverse Design and Probabilistic Acoustic Propagation," *Journal of Aircraft*, Vol. 43, No. 6, 2006, pp. 1815–1828. doi:10.2514/1.20457

[26] Darden, C., "Limitations of Linear Theory for Sonic Boom Calculations," *Journal of Aircraft*, Vol. 30, No. 3, 1993, pp. 309–314.

[27] Thomas, C., "Extrapolation of Sonic Boom Pressure Signatures by the Waveform Parameter Method," NASA TN D-6832, June 1972.

[28] Plotkin, K., "PCBoom3 Sonic Boom Prediction Model: Version 1.0e," Wyle Research, Rept. WR 95-22E, Oct. 1998.

[29] Makino, Y., Aoyama, T., Iwamiya, T., Watanuki, T., and Kubota, H., "Numerical Optimization of Fuselage Geometry to Modify Sonic-Boom Signature," *Journal of Aircraft*, Vol. 36, No. 4, 1999, pp. 668–674.

[30] Howe, D., "Sonic Boom Reduction Through the Use of Non-Axisymmetric Configuration Shaping," *41st Aerospace Sciences Meeting and Exhibit*, AIAA Paper 2003-929, Jan. 2003.

[31] Nadarajah, S., Jameson, A., and Alonso, J., "Sonic Boom Reduction Using an Adjoint Method for Wing-Body Configurations in Supersonic Flow," *9th AIAA/ISSMO Symposium on Multidisciplinary Analysis and Optimization*, AIAA Paper 2002-5547, Sept. 2002.

[32] Morgenstern, J., Arslan, A., Lyman, V., and Vadyak, J., "F-5 Shaped Sonic Boom Demonstrator's Persistence of Boom Shaping Reduction through Turbulence," *43rd AIAA Aerospace Sciences Meeting and Exhibit*, AIAA Paper 2005-0012, Jan. 2005.

[33] Pawlowski, J., Graham, D., Boccadoro, C., Coen, P., and Maglieri, D., "Origins and Overview of the Shaped Sonic Boom Demonstration Program," *43rd AIAA Aerospace Sciences Meeting and Exhibit*, AIAA Paper 2005-5, Jan. 2005.

[34] Farhat, C., Maute, K., Argrow, B., and Nikbay, M., "Shape Optimization Methodology for Reducing the Sonic Boom Initial Pressure Rise," *40th AIAA Aerospace Sciences Meeting and Exhibit*, AIAA Paper 2002-145, Jan. 2002.

[35] Alonso, J., Kroo, I., and Jameson, A., "Advanced Algorithms for Design and Optimization of Quiet Supersonic Platforms," *40th AIAA Aerospace Sciences Meeting and Exhibit*, AIAA Paper 2002-0144, Jan. 2002.

[36] Choi, S., Chung, H., and Alonso, J., "Design of Low-Boom Supersonic Business Jet with Evolutionary Algorithms Using Adaptive Unstructured Mesh Method," *45th AIAA/ASME/ASCE/AHS/ASC Structures, Structural Dynamics and Materials Conference*, AIAA Paper 2004-1758, April 2004.

[37] Choi, S., Alonso, J., Kroo, I., and Wintzer, M., "Multi-fidelity Design Optimization of Low-Boom Supersonic Business Jets," *10th AIAA/ISSMO Multidisciplinary Analysis and Optimization Conference*, AIAA Paper 2004-4371, Aug. 2004.

[38] Choi, S., Alonso, J., and Kroo, I., "Multi-Fidelity Design Optimization Studies for Supersonic Jets Using Surrogate Management Frame Method," *23rd AIAA Applied Aerodynamics Conference*, AIAA Paper 2005-5077, June 2005.

[39] Makino, Y., and Kroo, I., "Robust Objective Functions for Sonic-Boom Minimization," *Journal of Aircraft*, Vol. 43, No. 5, 2006, pp. 1301–1305. doi:10.2514/1.19442

[40] Harris, R., Jr., "Analysis and Correlation of Aircraft Wave Drag," NASA TM-X-947, March 1964.

[41] Carlson, H., and Mack, R., "Estimation of Wing Nonlinear Aerodynamic Characteristics at Supersonic Speeds," NASA TP-1718, 1986.

[42] Coen, P., "Development of a Computer Technique for the Prediction of Transport Aircraft Flight Profile Sonic Boom Signatures," M.S. Thesis, School of Engineering and Applied Science, George Washington Univ., Washington, D.C., March 1991.

[43] ModelCenter Ver. 6.0, Design Integration Software, Phoenix Integration, Blacksburg, VA, 2004.

[44] Li, W., Krist, S., and Campbell, R., "Transonic Airfoil Shape Optimization in Preliminary Design Environment," *Journal of Aircraft*, Vol. 43, No. 3, 2006, pp. 639–651. doi:10.2514/1.13921

[45] Plotkin, K., "Review of Sonic Boom Theory," *AIAA 12th Aeroacoustics Conference*, AIAA Paper 89-1105, April 1989.

[46] Carlson, H., Chu, J., Ozoroski, L., and McCullers, A., "Guide to AERO2S and WINGDES Computer Codes for Prediction and Minimization of Drag Due to Lift," NASA TP 3637, Nov. 1997.

[47] McCullers, A., "Flight Optimization System," NASA Langley Research Center, Hampton, VA, April 2001.

[48] Mangasarian, O., "Normal Solutions of Linear Programs," *Mathematical Programming Study*, Vol. 22, 1984, pp. 206–216.